TECHNISCHE UNIVERSITÄT WIEN

Diplomarbeit

Photo Physical Characterization of Red Emissive Fluorophores at Cryogenic Temperature

zur Erlangung des akademischen Grades

Diplom-Ingenieur

im Rahmen des Studiums

Master Biomedical Engineering

eingereicht von

Ying-Ju Chen
Matrikelnummer 11837557

ausgeführt am Institut für Angewandte Physik
der Fakultät für Physik der Technischen Universität Wien

Betreuer: Univ.Prof. Dipl.-Ing. Dr. Gerhard Schütz
Mitwirkung: Univ.-Ass. Dr. Arjun Sharma

Ort, Datum	(Unterschrift Verfasser)	(Unterschrift Betreuer)

Abstract

Single molecule localization microscopy (SMLM) is one of the popular and widely used method of super resolution optical fluorescence imaging techniques. It is a common tool for certain life science researches such as performing high resolution characterization of proteins structure or their distribution over cell plasma membrane. However, fast photo-bleaching rates and lesser blinking events of standard fluorophores at room temperature heavily limits the localization precision and resolution of such methods. In this regard, fluorescence measurements at cryogenic conditions have been observed to greatly improve the photostability of fluorophores, resulting in high photon collection from single molecules which in-turns improves the localization precision. However, insufficient details about the photophysics of fluorophores at cryogenic conditions may limit its application in super resolution imaging experiments. So, in this thesis we attempted to study certain photophysical properties of two important red emissive fluorophores at cryogenic conditions using our home-build cryostat and Widefield fluorescence microscope. A series of excitation power, exposure time, and excitation interval dependent measurements are performed to find an impact on a few fluorescence properties of these dyes such as the photobleaching, blinking and obtainable localization precision in SMLM. Combining the cryogenic treatment, our cryostat provided enhanced thermal and mechanical stability to the sample which can significantly prolong the life time of fluorescent specimen for several hours. On cooling down to 110K, we observed a large increases in the number of detected photons from single molecules of studied red dyes; Alexa fluor 647 and Atto 647N, which directly improves the attainable localization precision closer to the size of fluorophore.

Acknowledgements

I would like to express my appreciation to all people who supported me during my studies, especially the team of biophysics group of TU Wien on my diploma thesis.

First of all, I want to thank Prof. Gerhard Schütz for his supervision and support in my research. Thanks for inspiring me and giving me critical feedbacks on academic research. Secondly, my particular thanks for my Co-supervisor Arjun Sharma who guide me through all experimental details, presentation, and thesis writing. Thirdly, thanks Montserrat Lopez and Magdalena Schneider for organizing cryo group and helping me solving data analysis related questions.

In addition, I would like to thank Prof. Markus Valtiner, who provide me opportunities to reunite with my husband in Germany. Thanks for encouraging and giving me strong support to study in TU Wien. Besides, I would like to thank Katharina Schrom who teach me all knowledge of electric engineering relative courses to let me pass all challenging German exams.

Finally, to my dearest husband William, thanks for support and accompany me in every single day. Thanks for keeping encourage me when I feel depressed.

Contents

1 Introduction

1.1 Motivation and aim

Biophysical/biochemical processes are extremely efficient in energy utilization, conversion and often become the modeling system that inspires artificial engineering. In general, the complex biologic system involves countless delicate molecular level signaling, mass transportation, biochemical reactions as well as feedback control to balance all the processes at optimum conditions and remains prepared for reacting on any external impacts. For example, one simple biologic process such as balancing blood sugar level involves multi-layer of signal process with many functional proteins, receptors and feedback checking mechanism, which all happen in a very tiny volume of cell and thus becomes very challenging to probe/track by most of the present analytical techniques. Till now, such complex mechanisms aren't fully understood, particularly in molecular level. Therefore, being able to perform molecular level labelling/tracking is very essential for obtaining the whole reaction scheme of such complex biological processes. Placing a traceable tag onto targeting tissue/molecule is the most straight forward way of observing its behavior during a physiologic process[1]. For example, utilizing dyes to distinguish different functional tissues/structures under visible light range, such as Gram Stain[2]; or using radioactive tracer to label[3] specific chemicals/protein. Yet, the mention methods are not having enough lateral resolution to study molecular level processes.

In recent approach, fluorescence microscopy gradually become the leading trend of probing biophysical/biochemical processes due to its capability of performing single molecule imaging[4]. Fluorescence microscopy has broadly used to study the field of biochemical reactions, medical kinetics and biophysical processes due to its unique property of excitation/emission features. For example, fluorescent labeling helps to identify the cellular structure, multiple color staining[5] to study the distribution of targeting proteins[6] and tracking physiological process of a dye-labeled cell.[1] All of the achievements are based on the property of fluorescence emission, which is a slow but relatively faster process as compare to biological phenomenons. It is therefore possible to use fluorophores on tracking the motion of the labelled target within a physiological time frame. Additionally, fluorescence signal intensity can be significantly increased using high power laser, which greatly reduces the sampling time allowing to track fast kinetic process[7]. Another great advantage of using fluorescence microscope is the feature of Föster resonance energy transfer (FRET) between two fluorophores with matching emission/excitation energy gaps[8]. FRET typically occurs under the circumstance when two fluorophores get closer to a few nanometer separation, where the emitted fluorescence energy by one fluorophore can immediately absorbed by the nearby paired fluorophore, resulting in the change of emission wavelength. This feature is often used in single molecule kinetic study, such as defining the spring constant/vibration frequency of labelled molecules, studying protein aggregation as well as tracking the combination of two tagged molecule.

Although with the advance of analytical technique, maintaining the property of the specimens as close as one can to its natural status is highly demanding. To imagine biological structures in a near-native state in nanometer scale, the preservation of cells under such condition to keep it's physiological process normal become an especially important issue. In general, chemical fixation[9, 10] and cryofixation[11, 12] are the two widely used methods for performing in vitro fluorescence study. Chemical fixation utilizes agents to permeate tissues/cells and covalently bound to their certain biochemical composition of interest. However, even though the structure is maintained, the process may severally damage or change cellular properties so that it is not representative to the natural status. In contrast to chemical fixation, cryofixation can rapidly freeze the specimen, which immobilize and adequately preserve the completeness of biological structures. Thus, cryofixation greatly helps in the visualization of cellular ultrastructure, protein of interest and macromolecules in electron microscopy and conventional fluorescence microscopy [13, 14].

In recent decades, fluorescence microscopy has been improved to circumvent Abbe's diffraction limit (ca. 200 nm) to achieve better lateral resolution in optical image by using super resolution microscopy techniques such as SMLM, where the center of point spread function (PSF) is used to identify the lateral distribution of fluorophore with sub-nanometer precision[15, 16]. However, performance of such methods haven't been tested greatly under cryogenic conditions so far mainly due to certain unresolved challenges. For instance, requirement of low NA objective with cryostat leads to relatively poor optical resolution as compared to experiments at ambient environment. Besides low NA objective requirement, slow photo physics of fluorophores at cryogenic conditions further increases the measurement time to accumulate more photons for better localization precision which also leads to more sample drifts. Thus, better understanding of the photo physical properties of fluorophores at cryogenic conditions can be very helpful in maximizing their photon yields.

In this thesis, we attend to investigate the photo-physical properties of a few organic dyes under cryogenic condition. In particular, we will discuss the influence of different laser excitation parameters on the fluorescence performance of selected red fluorophores. Our parameters of interest are laser excitation power density, exposure time and image interval times, which are crucial to trigger fluorescence imaging processes. We will study effect of these parameters on certain photo physical properties of fluorophores such as photo bleaching, blinking in terms of On times and Off times and localization precision. The ultimate goal is to systematically develop a searching strategy to be able to collect as much photon as one can during a measurement time to improve the localization precision which can further be used for high resolution imaging. This approach will provide us a broad view to optimize the operational condition, and therefore gaining an in-depth understanding of the interaction between light and fluorophore under cryogenic condition.

1.2 Fluorescence: Science and application

Fluorophore is a molecule featured with specific light absorption characteristic as well as an associated re-emission process with a longer wavelength also known as fluorescence. Fig. 1 shows an example of the excitation and emission spectrum of a fluorophore. The wavelength of fluorescence or emission light is usually determined by the chemical properties, local temperature and the chemical environment of the fluorophore[17]. Fluorophores generally contain several aromatic groups or cyclic compound with several π bonds i.e. a conjugated electronic structure. This enables the molecule absorb a photon of certain range of wavelength, mostly in the UV-visible light range (i.e. λ = 300-700 nm) followed by release of lesser energy photon, a phenomenon called as fluorescence.

A complete process of fluorescence can easily be understood with the help of Jablonski diagram, as shown in the Fig. 2. Fluorophore first gets excited from its ground singlet state (S_0) to first excited singlet state (S_1) by absorbing the excitation photons of resonating energy. The Planck relationship shows the energy requirement of electronic transition within Jablonski diagram that is given by a quantum of photons with the proper frquency:[17]

$$E = h\upsilon = hc/\lambda \tag{1}$$

E = the energy of electronic transition.
h = the Planck's constant. (6.626×10^{-34} m^2 kg/s).
υ = the frequency.
c = the speed of light. (3×10^8 m/s).
λ = the wavelength.

Shortly after the excitation, the excess energy can be partially dissipated in the same electronic level by means of heat dissipation via vibrational relaxation, also known as internal conversion (IC). But even after IC, molecules at S_1 state are still not stable. Therefore, within few nanoseconds, majority of the molecules release their energy in form of radiative transition to come back to the ground state, the phenomenon called as fluorescence emission. As fluorophore consumes some of the energy of excitation photon for vibrational relaxation, the fluorescence photon always appears with higher wavelengths, the reason for red shifted emission spectrum. In general, difference between the maximum excitation and emission wavelength is termed as stocks shift. When fluorophore consist of more extended conjugated electron systems, the energy difference (band gap) between the highest occupied molecular orbital (HOMO) and the lowest unoccupied molecular orbital (LUMO) will become smaller, which results in even longer wavelength of emission light, that is more stocks shift.

Being able to emit photons like a point source, fluorophore can be used as labelling agents in light microscopy to identify or locate an object. Thus, fluorescent dyes are now been used for

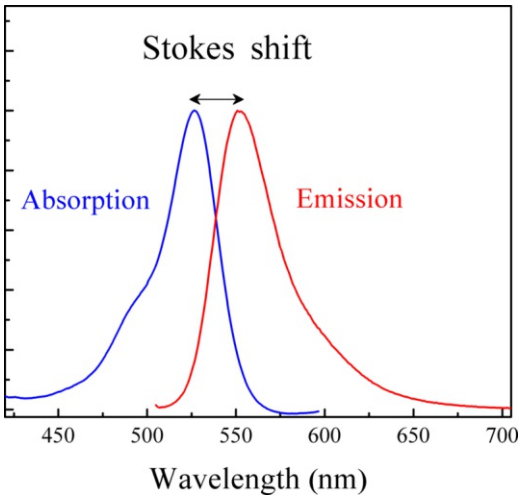

Figure 1: Absorption and emission spectra of a fluorophore with stokes shift. The blue and red lines show the absorption and emission spectra of a dye respectively.[21]

staining various cell structures, a tracer or marker of bio-molecules in liquid, and for site specific labeling of macromolecules by covalent bonding or immunolabeling.[18]

But, fluorescence emission is just one of many relaxation processes. Beside fluorescence or relaxation via heat dissipation, a very small portion of fluorophores (ca. 0.1 %) can also relax through either non-fluorescent triplet state or via extremely long lived dark states. Depending upon lifetime of different states, fluorophore eventually returns to the ground state (S_0) in the end and re-enter the ordinary excitation/emission cycle[19]. Such longer de-excitation can occurs in the timescales of a few microseconds (lifetimes for triplet states) to millisecond or seconds (lifetime of long lived dark states). Both of these transitions appears like a blink of fluorophores in there respective time frame and can be observed using a photo detector of suitable temporal resolution. This complete switching of fluorophores from On to off states helps in determining their individuality in a complex environment. So, this natural photo blinking property of fluorophores plays a crucial role in differentiating neighbouring molecules in single molecule localization based super resolution microscopy[20].

But, the fluorescence process is not always reversible. Another possibility is the permanent photo bleaching of dyes, which is defined as the loss of fluorescence characteristic of fluorophores after certain number of excitation emission cycles. This mainly depends upon the excitation power and exposure time of excitation beam. Photobleaching may result from various phenomenon triggered by photo excitation of fluorophore such as conformational changes (e.g. the break down of the covalent bonds), isomerization, irreversible destructive reaction to change the excitation/emission features between the fluorophores and the surrounding molecules, or structural damage due to very long illumination of light. All such processes requires either physical movement of excited fluorophore or its interactions with surroundings. Therefore, handling fluorophores under certain inert environment or freezing them under cryogenic conditions can help in efficiently reducing the photo bleaching rates of most fluorophores.

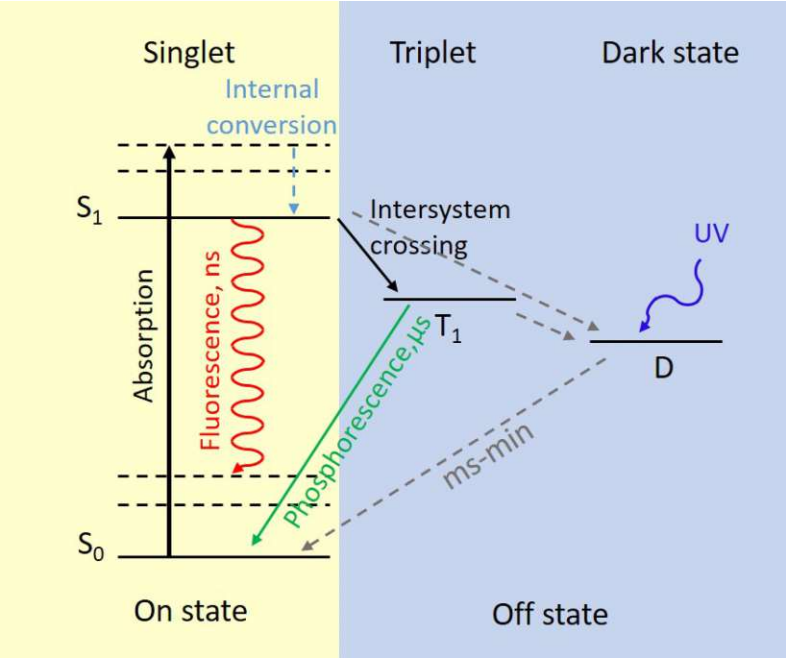

Figure 2: Jablonski Diagram of fluorophores blinking. On excitation, fluorophores transitions to the first excited singlet state (S_1) and then fluorescence back to the ground state (S_0) after internal conversion process. A portion of fluorophores may relax to triplet or dark state via intersystem crossing, which represents Off state of fluorescent dyes.[19]

In general, there are a few characteristics of fluorophores which are used to identify its applicability for applications in microscopy. Those major characteristics of fluorophores are:

Range of excitation and emission wavelength (nanometer): Ideally, the excitation and emission spectrum of fluorophores should fall under the visible range of light spectrum for its applicability with bio specimens.

Molar absorption coefficient or molar extinction coefficient ($M^{-1}cm^{-1}$): A measured value of how a matter attenuates light with a certain wavelength.

According to the Beer–Lambert law, light absorbance depends upon the concentration of absorbent and path length of light while inside the absorbent. Mathematically,

$$A = \varepsilon[c]d \tag{2}$$

A= the absorbance of a substance.

ε = the molar absorption coefficient of that material.

[c]= the molar concentration of that material.

d= the distance of optical path length.

Quantum yield: A measured value of the efficiency of photon emission that is defined as the ratio of the number of emitted photons to the number of absorbed photons.

Brightness: The product of molar extinction coefficient and the quantum yield.

Stokes shift: The difference between maximum excitation and emission spectra as shown in Fig. 1.

Photo-sensitivity of photo-toxicity: Less photosensitive fluorophores are usually preferred due to the requirement of their longer appearance during the analysis.

Blinking: Further existence of long lived (≥ ms) dark states of fluorophores ensures the presence of long time photo blinking: a crucial parameter of high resolution imaging. This parameter is generally quantified in terms of the On times and Off times of fluorophores. On times of fluorophores defines how long a dye can continuously emit fluorescence (bright state) without blinking, and Off times shows how long fluorophores remains in the Off (dark) state. On and Off times properties depends on excitation laser power and distinct organic dyes.[22]

1.2.1 Fluorescence microscopy

Fluorescence microscope is an optical microscope that utilizes emitted fluorescence light to image the object for example in case of Widefield fluorescence or Confocal microscopes. Most of such microscopes work under the epifluorescence mode to minimize the collection of scattered excitation light. In this configuration fluorescence is collected by the same objective which is used for the excitation of sample as shown in Fig. 3. Fluorescence microscopy plays an important role on biological and biomedical sciences and provides noninvasive imaging of biological cells.[23] The principle of fluorescence microscopy is that the specimen labelled with one or multiple fluorophores is irradiated by a specific wavelength of light in order to collect the fluorescence signals from fluorophores and utilizes it to identify or locate the position of the specific specimen in sample. Benefited from the specific emission wavelength and completely dark background, the fluorescence microscopy can therefore be used to perform high contrast imaging, specific target identification and quantitative labelling. Also due to high selectivity of chemical attachments, fluorescence microscopy is distinctively used to detect and identify discrete molecules, and observe intra- and inter-molecular interactions with high temporal and spatial resolution[23].

A typical fluorescence microscope consists of an excitation light source, an objective and a camera or single photon detectors. Various optical elements such as a cleanup filter for lasers, a dichroic mirror and set of emission filters are additionally used as shown in the Fig. 3.

Light Source: The conventional light source of a fluorescence microscope are usually high-power LEDs, dye lasers, xenon arc lamp or mercury-vapor lamp. Based on the type of experiment, either pulsed or continues mode of excitation are used.

Cleanup filter (or excitation filter): These filters are used to selectively pass a narrow band of visible light spectrum and block other unwanted wavelengths coming out of light source.

Dichroic mirror (DM): These are usually long pass filters, used to separate fluorescence light from the scattered excitation beam. These mirrors are designed to have high reflectively to light with wavelength shorter than a given threshold, where the light with longer wavelength can be transmitted.

Objective Microscope objective is the heart of the system as it majorly determines the quality and magnification of specimens. It consists of a complex arrangements of several optical lenses

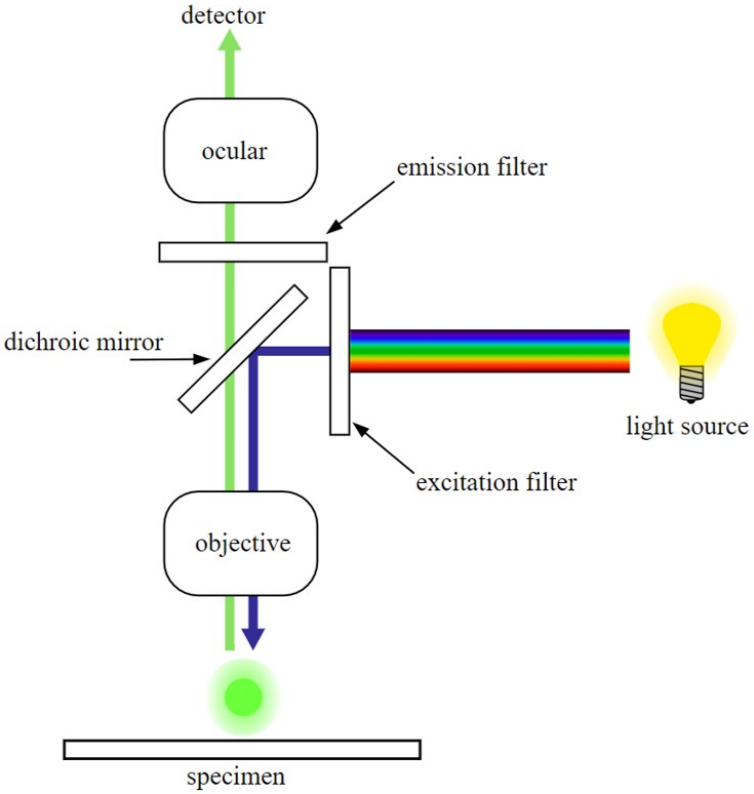

Figure 3: Schematic of operation principal of an epifluorescence microscope [24]. The filtered light beam is reflected by the dichroic mirror and then focused by the objective to irradiate on Specimen. Emitted fluorescence from the specimen is collected by the same objective, and then transmit through the dichroic mirror, emission filter and finally arrives the photo detector,

to focus the excitation laser beam onto the specimen to trigger the fluorescence emission, and simultaneously collect the emitted fluorescence from its focal plane. Microscope objectives are characterized by two important parameters i.e. (1) magnification and (2) numerical aperture(NA). Both these parameters contribute equally to determine the overall resolution of an optical microscope. Objective magnification along with the pixel size of camera determines the camera resolution whereas numerical aperture defines optical resolution of the setup.

Emission filter (EF): Additional emission filters are used after filtering the fluorescence light by dichroic mirrors to further remove any remaining scattered signal which further improves signal to noise ratio.

Detector: Depending upon the type of experiment, various type of photo detectors can be used in fluorescence microscopy. In case of fast fluorescence imaging, Charge Coupled Devices (CCD) or scientific Complementary Metal Oxide Semiconductors (complex arrangements) are generally used. The choice of camera depends on various factors such as the required frame-rate, field of view and resolution etc. In present work, we have used a 4.2MP sCMOS camera for our photophysical analyses of single dye molecules.

1.2.2 The resolution limit of conventional light microscope

Optical microscope typically utilizes visible light (range of 380-700 nm) as its light source to produce magnified images of tiny objects through a designed optical train. Through the increasing demand of the optical resolution in many applications, optical microscope has been integrated with more complicated designs to challenge the physical resolution limit of visible light imaging. Typically, the resolution (also known as resolving power) of a microscope can be defined as the ratio of the shortest distance between two distinguishable points to their full width of half maximum (FWHM). But, the resolution of the optical microscope is limited by the wavelength of the used light source, where any sub-wavelength features are not optically resolvable due to the Abbe's diffraction limit.

Diffraction is a general feature of scattering observed after an interaction of electromagnetic wave with material. In optical microscope, it is a cumulative feature after light passes through optical elements, such as iris, aperture and slit. Therefore, diffraction of light is extremely critical to the resolution (resolving power) of any optical instrument (for instance: cameras, microscopes, and eye).

In optics, diffraction causes a point object not being as a point, but as an Airy disk and Airy pattern (lateral optical image of the point) as shown in Fig. 4(a). Ernst Abbe found the diffraction limit[25] of optical microscopes in 1873 According to that principle a light beam passing through a medium with refractive index of n and converging to a point with half angle θ, will have a smallest resolvable distance (D) as

$$D = \frac{\lambda}{2nsin\theta} = \frac{\lambda}{2NA} \tag{3}$$

λ = wavelength of emitted light.
NA = the numerical aperture of objective.
n = refractive index of the medium between specimen and front lens of the objective.
θ = half angular aperture of the objective lens.

According to this equation, the optical resolution of microscopes can be improved either by increasing the numerical aperture of objective or by selecting fluorophores with shorter emission wavelengths. But, even with that the resolution of optical microscope is still restricted to around 200-250nm. The Rayleigh criterion shows that two points in the image can be separated if the maximum of the first point spread function (PSF) overlaps minimum of the second PSF as shown as Fig. 4(b)-(d). For separation of two Airy disk, the Rayleigh criterion indicates the minimum resolvable distance (D):

$$D = \frac{0.61\lambda}{2NA} \tag{4}$$

If the distance between two points is less than this value, they cannot be laterally resolved.

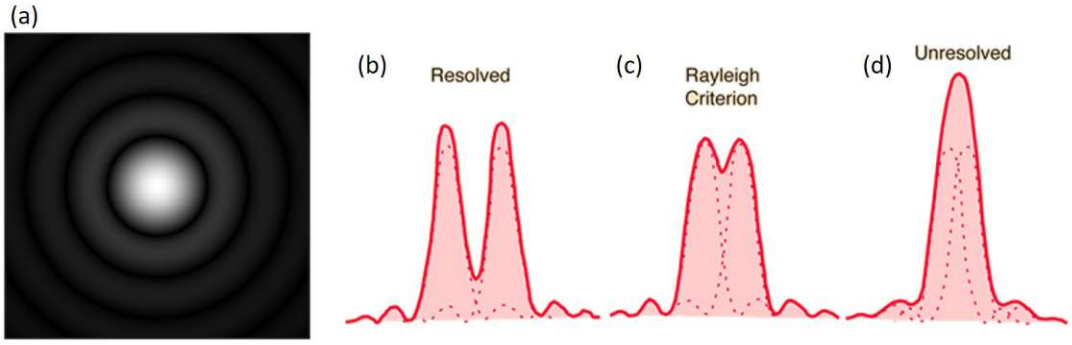

Figure 4: (a) Example of an Airy disk, which consist of bright circular aperture in the central region with series of concentric rings. Illustration of the spatial resolution between two points of (b) well-resolved, (c) Rayleigh criterion: the minimum distance between two distinguishable points, and (d) not resolvable cases[26, 27].

Imaging a point object gives the PSF, which is a three-dimensional diffraction pattern of light transmitted to the image plane through a higher numerical aperture of objective lens.

Although the physical limitation is coming from the nature of light, there are many experimental and mathematical approaches that are able to overcome this limit for studying sub-wavelength features.

1.2.3 Super-resolution microscopy

In last two decades, various super-resolution microscopy methods have been developed and used to overcome the diffraction limit of conventional light microscope and achieved higher resolution fluorescence images. The two major far-field super-resolution imaging methods are deterministic and stochastic super-resolution. The deterministic super-resolution imaging method includes stimulated emission depletion (STED)[28] and structured illumination microscopy (SIM)[29]. Details of these methods are beyond the scope of present thesis.

The stochastic super-resolution imaging method applies the precise positioning of single molecules by utilising the on/Off switching property of fluorophores. Methods like photoactivated localization microscopy (PALM)[30], stochastic optical reconstruction microscopy (STORM)[31] works on the same principle and provides very high spatial resolution [23]. These methods are generally categorized as single-molecule localization microscopy (SMLM).

1.2.4 Single molecule localization microscopy (SMLM)

Single molecule localization microscopy can locate the position of individual fluorophores with precision over the Abbe's diffraction limit (ca. 200 nm), which is essential for obtaining a high resolution image with dye-labeled specimen. As shown in Fig. 5, the flow chart describes the procedure of acquiring high resolution SMLM image starting from raw data sampling. In normal conventional image, diffraction limit of the light constrain the image resolution. However, benefited from the photo-switching (photo-blinking) of standard fluorophores or even fluorescent

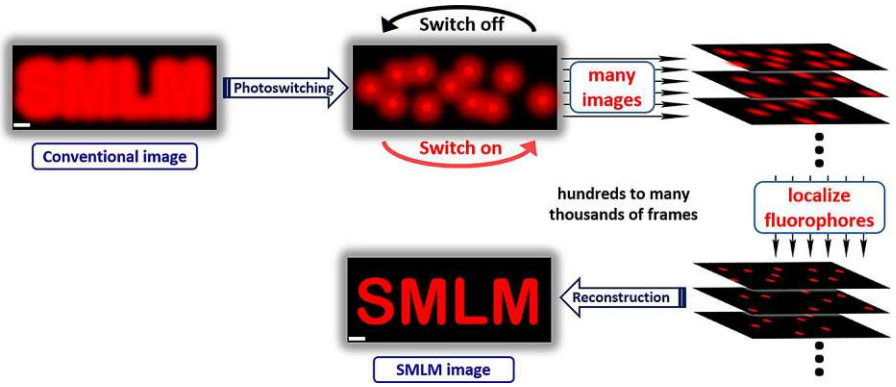

Figure 5: Flow chart of the principle of single molecule localization microscopy (SMLM). Using the photo-switching properties of fluorescent molecules, a high resolution SMLM image can be reconstructed from accumulating recorded frames, where the more the frame collected the higher resolution can be achieved[32].

proteins, a high resolution image can be obtained with additional post image processes. Fig. 5 demonstrates that the accumulation of a huge number of images (frames) will be able to enhance the photon counts per localized fluorophore, which leads to a higher localization precision. In addition, the active fluorescent molecules should be well and sparse-distributed in each frame, as well as with photo-blinking (photo-switching) features. This is the key concept of achieving sub-wavelength resolution in SMLM. It is therefore advantageous to use small fluorophores (1 nm) or fluorescent proteins (4 nm) as point emitters to label biological targets (e.g. antibodies and living cells) for acquiring their spatial distribution information with high localization precision.

The localization precision (σ_{loc}) plays an important role on the quality of a SMLM image and determines the reachable spatial resolution. This quantity shows how precise the position of a single fluorescent molecules can be located. Several methods are employed to quantify the localization precision. A common approach is fitting the fluorescence spots on acquired image frame using a set of PSF, which consist of a two dimensional Gaussian function. It will effectively determine the center of fluorescent emitters with accurate coordinate in a frame.[33] Therefore, the localization precision is crucial on interpretation of the SMLM image resolution and quantitative analysis. The following equation defines localization precision (σ_{loc}) [34]:

$$\sigma_{\text{loc}} = \frac{\sigma_{\text{psf}}}{\sqrt{N}} = \frac{0.25\lambda}{NA\sqrt{N}} \tag{5}$$

σ_{psf} = the full width at half maximum(FWHM) of point spread function(PSF),

λ = emission wavelength,

N = amount of collected photons,

NA = numerical aperture of the objective.

The localization precision is determined by the number of detected photons and the FWHM of the point spread function (PSF) for trivial background noise[23, 34]. Therefore higher localization precision can be achieved by either increasing numerical aperture of objective[35] which increases

the fluorescence photon collection efficiency or by increasing the accumulated photon counts by stabilizing fluorophores against excitation light under cryogenic conditions [34, 36].

1.3 Fluorophores at cryogenic temperatures

As discussed in previous sections, slower photo bleaching of dyes is a crucial parameter for efficient single-molecule fluorescence imaging [37, 38]. There can be various factors responsible for permanent bleaching of fluorophores at ambient conditions (discussed above). However, as most of these factors require molecular motion of excited fluorophores, freezing the sample down to cryogenic conditions can decrease the probability of its interaction with surroundings. This indeed can enhances the photo stability of fluorophores resulting in higher photon counts per molecule and so the better localization precision [16]. Hulleman et al. recently revealed that the lateral resolution of red fluorophore can be improved by 10 fold under cryogenic condition, where a photon yield of 3.5-11 x 10^6 can be achieved before bleaching. These high photon yields corresponds to a theoretical localization precision of 0.1 nm [34].

However, it is not only the localization precision which defines achievable resolution but also the blinking behaviour of the fluorophores. In ideal cases, Off times of fluorophores should be sufficiently higher (50 to 100 times) than their On times in order to differentiate molecules under SMLM. Various chemical induced blinking methods such as use of STORM buffer are used in room temperature SMLM imaging experiments which creates additional dark states for fluorophores leading to higher Off times and thus better achievable resolution. But as such methods can not be used under cryogenic conditions therefore we are limited to use the natural blinking properties of dyes which generally express low Off times. In such case, single molecule localization methods at cryogenic condition may need additional parameters to differentiate nearby molecules. For example, Weisenburger et al. have implemented a 3D cryogenic optical localization method (COLD) to resolve protein structure in Angstrom resolution by using the fluorescence intensity filtering approach to localize multiple fluorophore-labeling[36]. Similarly, Böning et al. have exploited polarized and periodical modulation of laser source to distinguish nearby molecules via distinct dipole orientation and induce fluorophores photo-switching under cryogenic temperature[22]. In addition, multi colour labelling/detection can also be used for single molecule identification provided that the system is well designed for minimal chromatic aberrations.

Besides reduced blinking efficiencies, experiments at cryogenic temperature requires very high vacuum around the sample in order to avoid any heat exchange with the surroundings. Thus, standard high NA immersive objectives can not be used under such arrangements and objectives can not be in direct contact with sample. Therefore only air objectives with low NA can be used in conventional cryo fluorescence microscopy setups. These objectives heavily reduces the photon collection efficiencies as compare to immersive objectives and thus requires very long data acquisition time to obtain similar photon yields. Here, cryogenic condition helps keeping the sample active for longer time due to enhanced photostability but longer measurements often

struggle with huge sample drifts. Therefore a proper drift corrections in x,y and z need to be done before the photo physical analyses of specimen images. X and y drift can be easily corrected with the help of fiducial markers during post processing of image. But sample drifts in z should be minimized during the experiments with the help of an active focus hold system.

2 Methods and Materials

2.1 Cryo-fluorescence microscope setup

In this thesis, all cryogenic fluorescence microscopy experiments were performed using our home-build cryostat and wide-field fluorescence microscopy setup. The cryostat design is inspired from one by Prof. J. Enderlein's group [39]. Fig. 6 and 7 represents the schematic and real arrangement of our cryo fluorescence microscopy setup.

Here, we utilize dual laser system providing orthogonal polarization of 640 nm red excitation laser sources for selective excitation of fluorophores which helps in identifying a nice single molecule distribution in our samples. The polarization direction of two laser sources are first conditioned using cleanup filter (CF) and wave plate (WP), then redirected into the same optical path with a polarizing beam splitter (BS). BS is placed inversely in this setup which reflects one polarized laser and transmit other resulting in redirection of both lasers in same direction. Then a telescopic lens system is used to focus the beam onto the back focal plane of the air objective (60x, 0.7 NA) resulting in the generation of well collimated excitation beam from the objective which then used to excite the sample placed inside the cryostat. The fluorescence from the sample is then collected by same objective and first filtered through the dichroic mirror. Here, dichroic mirror (DM) is used as a long pass filter which reflects the excitation light and transmit the fluorescence. The divergent fluorescence light is then further filtered by additional emission filters and focused onto the camera chip with the help of tube lens (TuL). In our setup, a 4.2MP sCMOS (scientific complementary metal-oxide-semiconductor) camera has been used with the pixel size of 6.5 micron. Combined with 60x magnification objective it provides the camera resolution of 108 nm (i.e. effective pixel size in images). But due to 0.7 NA of current objective, we get only around 470 nm of optical resolution for 655nm emission wavelength .

During the measurement, the specimen is cooled using liquid nitrogen (77K) under high vacuum (ca. 10^{-5} mbar) to prolong its fluorescence durability. In general, our setup can maintain this high vacuum and temperature for more than 15 hrs while filled with liquid nitrogen. This enables us to perform long time measurements with ease. Alternative excitation of sample with orthogonal polarized light helps us identifying the single molecule distributions in the sample as they blink over switching the lasers. For any quantitative experiments, it is important that both lasers have same intensities/power. Thus, laser power is recorded on top of the objective and divided with illumination area (6.36×10^{-5} cm^2) to determine laser densities in W/cm^2.

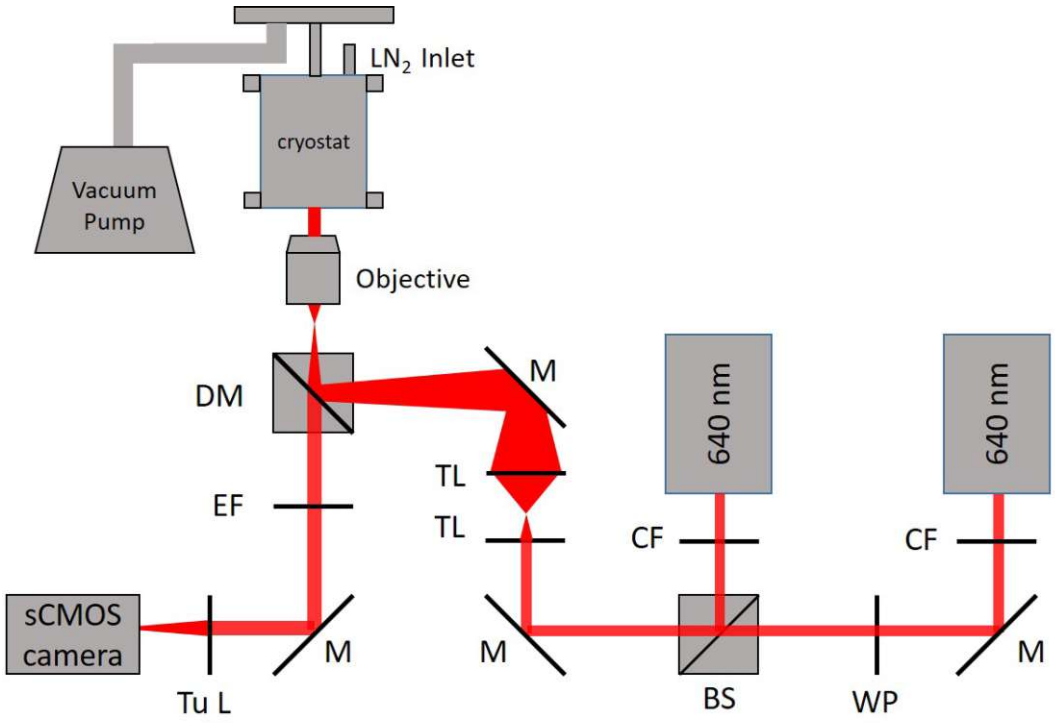

Figure 6: Illustration of the used cryo-Single molecular localization microscope setup, where the abbreviations used are listed as following: BS polarizing Beam Splitter, DM Dichroic Mirror, M Mirror, TL Telescope lens, EF Emission Filter , CF Cleanup Filter , WP Wave plate and Tu L Tube lens, sCMOS camera scientific complementary metal-oxide-semiconductor camera.

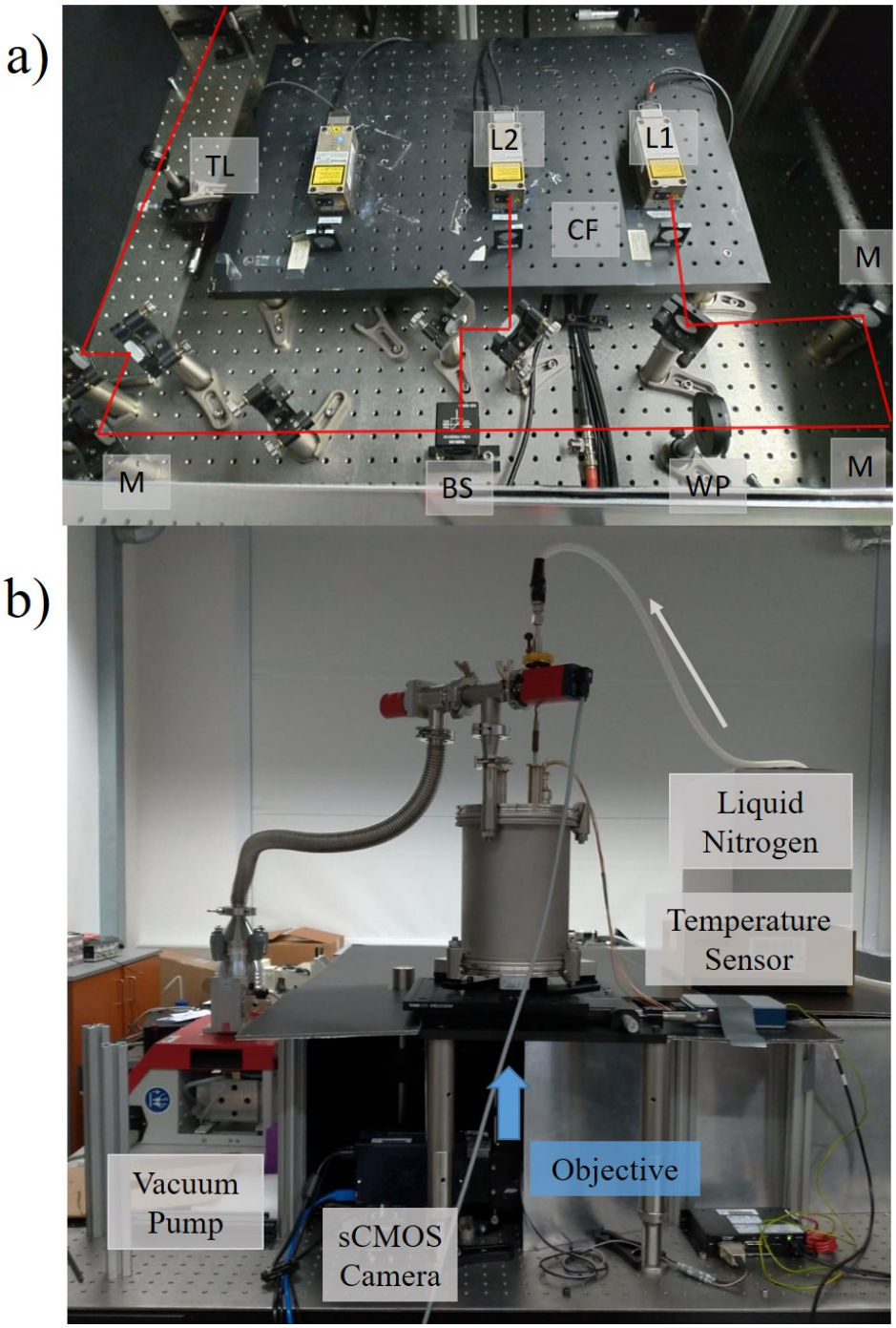

Figure 7: The single molecule localization microscrope setup (a) Optical train arrangement with simulated optical path. L1 and L2 are two red orthogonal lasers with 640 nm output, CF: cleanup filter, M: mirror, WP: wave plate, BS: beam splitter and TL: telescope lenses.(b) The moment of cryostat while adding liquid nitrogen and pumping. The temperature sensor and pressure sensor monitor the variation of temperature and pressure change. Objective is under cryostat and the resulted emission signals pass through objective and dichroic mirror and are detected by camera.

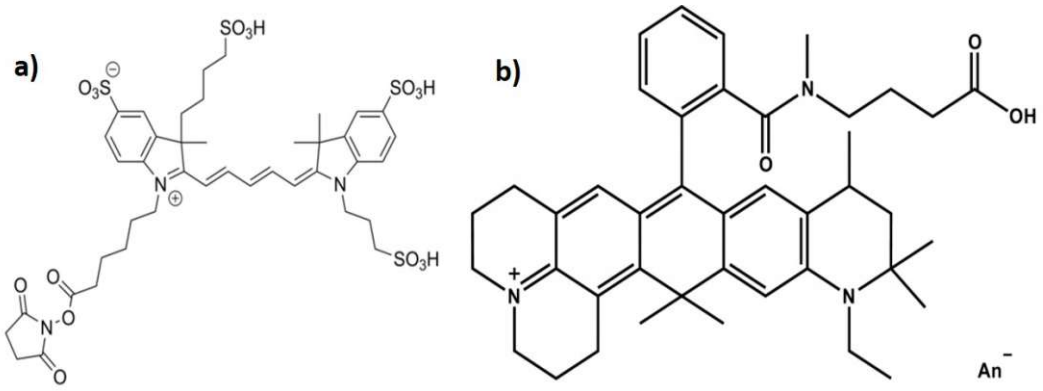

Figure 8: Chemical structure of studied dyes: (a) Alexa fluor 647 (AF 647)[40] and (b) Atto 647N[41], with excitation/emission characteristics of 640/668 and 644/669 nm respectively.

2.2 Fluorophores

In present thesis, we have chosen fluorophores with higher fluorescence quantum yields, extinction coefficient and so high brightness. In particular, Alexa fluor 647 (streptavidine conjugate) and Atto 647N (NHS ester conjugate) are studied due to their wide range of applications in fluorescence microscopy. Alexa Fluor 647 (AF 647) is a sort of cyanine derivative as shown in Fig.8 (a) which can be excited by red laser (640 nm) and has maximum emission at 668 nm. AF 647 has high molar extinction coefficient close to 270,000 $M^{-1}cm^{-1}$ and quantum yield of 0.33. AF 647 is widely used to fluorescent labeling with high sensitivity and flow cytometry, and can be conjugated to proteins, antibodies and various cells for specific labeling and detection.

On the other hand, Atto 647N (AT 647N) is also a red fluorescent dye (Fig.8 (b)) with maximum excitation wavelength 644 nm and maximum emission wavelength 669 nm. Atto 647N has excellent quantum yield of 0.65 but slightly lower extinction coefficient (150,000 $M^{-1}cm^{-1}$) than AF 647, making it almost similar bright as AF 647. It also has good solubility in polar solvents making it very useful for labeling proteins, DNA or RNA structures.

2.3 Experimental details

2.3.1 Sample preparation

Stock samples (concentration ca. 10 μM) of studied dyes were first taken out from -20 degree Celsius refrigerator and kept outside for some time until it reaches the room temperature (298K). Both dyes were then diluted roughly up to 5 nM using 1x PBS buffer (Phosphate buffer Saline). Diluted samples was then sonicated in water for around seven minutes to dissolve any present molecule clusters in the mixture. In order to prevent dyes from degradation by surrounding lights, the whole sample preparation procedure was carried out under very low illumination environment.

Meanwhile, a round shape glass coverslip with diameter 12 mm and thickness 0.13 mm was cleaned by plasma clean for more than 10 minutes to remove all organic impurities on surface[42].

Plasma cleaner uses energetic plasma made from ionized gaseous species which reacts with hydrocarbons present on the surface of specimen (glass) via physical ablation or chemical reaction.

Then, 2 to 4 μl of 5 nM dye solution was gently dropped on the cleaned glass coverslip which spread nicely due to well charged hydrophilic surface of glass. Then, we waited for around five minutes to let the dye molecules attach nicely to the surface. Then we carefully dried the remaining solution droplets by soft Argon stream. At this moment, we see dried salt residue from PBS on the glass coverslip as well which could interfere with our imaging. So, we washed the sample coverslip with roughly 200 μl of ultra pure water which also significantly reduces the sample densities. Therefore, we optimized the initial sample concentration to get nice single molecule distribution which turned out to be in range of 5-10 nM. Washed sample was then further dried under soft argon stream and was transferred to the oxygen free copper made sample holder of cryostat (Fig. 9 (b)).

Although, our sample holder of cryostat is mainly designed for TEM grids (diameter 3 mm), it can also hold a 12 mm glass coverslip on top. The sample glass is then covered with magnetic stainless steel lid which holds the sample in between via magnetic attachment to installed magnets inside sample holder. In this arrangement, our dye sample can be viewed/imaged through tiny holes in the lid. After that, sample holder was gently transferred to the bottom of the cryostat which further attaches there by magnets. A covering lid with a 0.7 mm thick sapphire glass window was then used to seal the sample holder loading chamber of the cryostat to secure the quality of the vacuum. When sample loading is completed, the cryostat is re-position as shown in Fig. 9 (a) on a translation stage, where the objective and whole optical train is underneath. After that, we connected cryostat to vacuum pump which was required to isolate the cold N_2 tank and sample from the outer body of cryostat. When internal pressure drops down to 10 mPa, we started filling the liquid nitrogen (77 k) inside the cryostat. At this moment, pressure drops further to 1 mPa and sample reaches temperature around 110 K within 6-7 minutes i.e. below the glass transition temperature of water (135K). We then additionally waited for one hour for the thermal fluctuation to get minimized. Once the temperature and pressure are minimized, the vacuum inside the cryostat was sealed and pump was disconnected to prevent the influence of mechanical vibration. In this way, our cryostat provide excellent thermal conductivity and mechanical stability that is ideal for cryogenic experiments. At this moment, we start to perform searching of area of interest and focus adjustment, as well as monitoring such as the laser status, temperature stability and change of background pressure.

2.3.2 Data acquisition

To keep dyes under optimum condition (unbleached), the laser was only switched on during sample search, focus and data acquisition. As mentioned above, in this thesis we are aiming to study the fluorescence performance of dyes under the variation of certain imaging parameters such as excitation laser power, exposure time and pulse intervals. We have used laser power

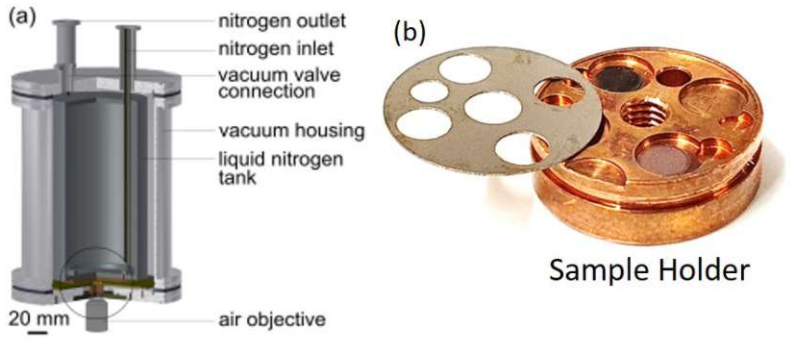

Figure 9: (a) Cross section of the used cryostat [39], where the sample mount is positioned at the bottom. The cryostat consist of a cooling tubing, which delivers liquid nitrogen directly to the backside of the sample holder for cooling. To prevent the heat exchange, the inner chamber is pumped into high vacuum during the experiment. (b) photo of used copper sample holder and lid[39, 43].

ranging from 0.1 kW/cm^2 to 1.0 kW/cm^2, continues exposure time from 50 ms to 2s and pulse intervals from 10 ms to 200 ms. It is worth mentioning that the continues excitation of sample should be avoided in fluorescence microscopy as it brings faster photo bleaching and local heating of the sample. Therefore, an interval of few ms between two laser pulses is used to maintain the sample for longer measurements.

The results are acquired in format of TIF image from sCMOS camera with its sampling frequency synchronized with the laser source pulse frequency. This ensures that the even and odd frame number are contributed from two laser sources separately. Being frozen under cryogenic conditions, fluorophores ensures fixed excitation dipole moment which can only be excited with an appropriate polarization of light. Thus, the use of two lasers with orthogonal polarization here helped us in identifying nice distribution of single molecules on cover glass as in such case most of the single molecules appear only in even or odd frames[44]. For example, Fig. 10 represents two consecutive raw images of AF647 dye molecules taken by excitation with two orthogonal polarized laser. Appearance/disappearance of molecules between these frames strongly indicate nice distribution of single molecules on coverslip. Using this approach, we selected only those samples and areas which had nice single molecule distribution.

Acquired images were then analyzed to further characterize the number of fluorescence events and the photon counts during the given exposure time. Here, we used SMLM approach to record the appearance and brightness of individual molecules with respect to various parameters. For this, we used software ImageJ with ThunderSTORM plugin. All used parameters to perform single molecule localization and drift correction are shown in the appendix.

Here, ThunderSTORM fits the point spread function (PSF) of individual fluorophore with integrated Gaussian function and locates the maxima as localization of the fluorophore. Number of such fits in a frame then can be counted as number of localizations or number of molecules. However, comparing the molecular size (range of a few nanometers) to the optical resolution limit of 400-500 nanometers, it is not yet straight forward to correlate the number of fitted PSF to

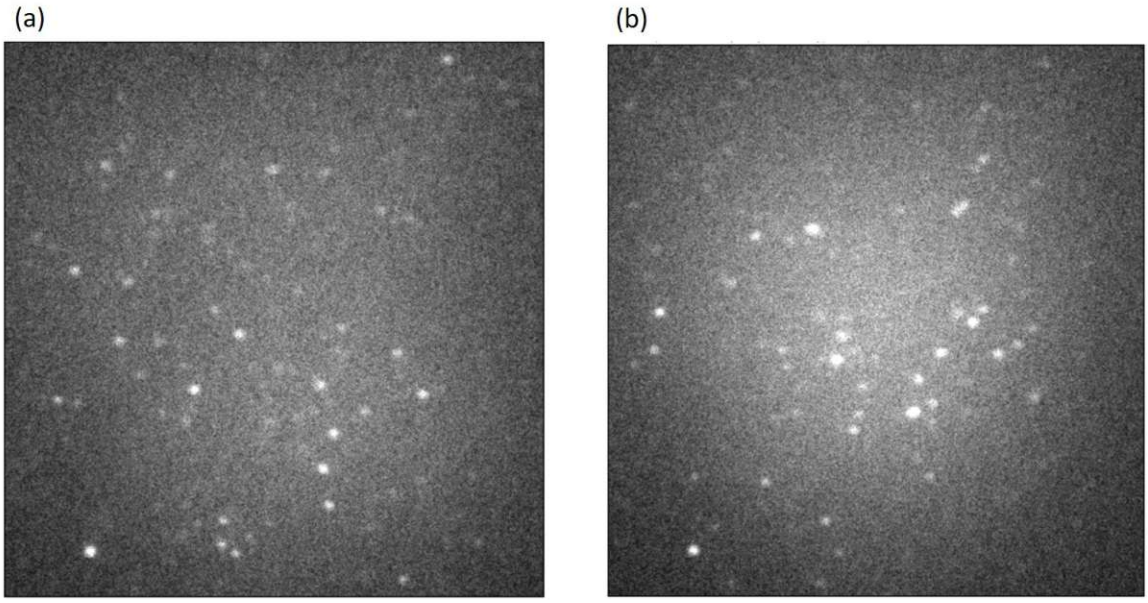

Figure 10: Odd frame and even frame under two orthogonal lasers irradiation in the same region of interest. Single frame photo from region of interest at (a)frame number = 1 and (b) frame number = 2. It can be distinguishable that fluorescent signals are single molecule or cluster by irradiation of two perpendicular lasers. The demonstrated results are from AF 647 dye with laser power density of 0.4 kW/cm^2, exposure time 100 ms and interval of 10 ms at 110 K.

number of fluorophore, where closely aggregated fluorophore molecules may result as one PSF. Thus, number of localization can be considered similar to the number of molecules in frame only in case of low concentration system with low molecular aggregation characteristics or in other way under nice single molecule distribution on glass. As mentioned before, we only used those ares for analyses which were confirmed to have nice single molecule distributions.

After successful localization of individual fluorophores in all frames, the analysis software tracks the coordinate change of 20 % of the localizations to conduct drift compensation. The drift will only be recognized when all the monitored localizations moves synchronously in same direction and same displacement. Fig. 11(a) shows the tracked systematic drift over a period of experiment. Here in this exemplary experiment, the overall drift over the whole collected 3000 frames (5 minutes) shows maximum of 100 nm, indicating the excellent stability provided by our home build crostat and microscopy system. Fig.11(b) represents the super resolution image obtained after stacking all drift corrected frames. Additionally, we used density filters to filter the noise in obtained frames. After density filtering, only those localization's were saved which were appearing at least five times with 50 nm regime.

2.3.3 Data analysis

After drift correction and filtering, the individual frame localization data was saved as an excel file including all important information such as frame number, localization, collected photons, standard deviation and uncertainty. This data was then used to study various photo physical

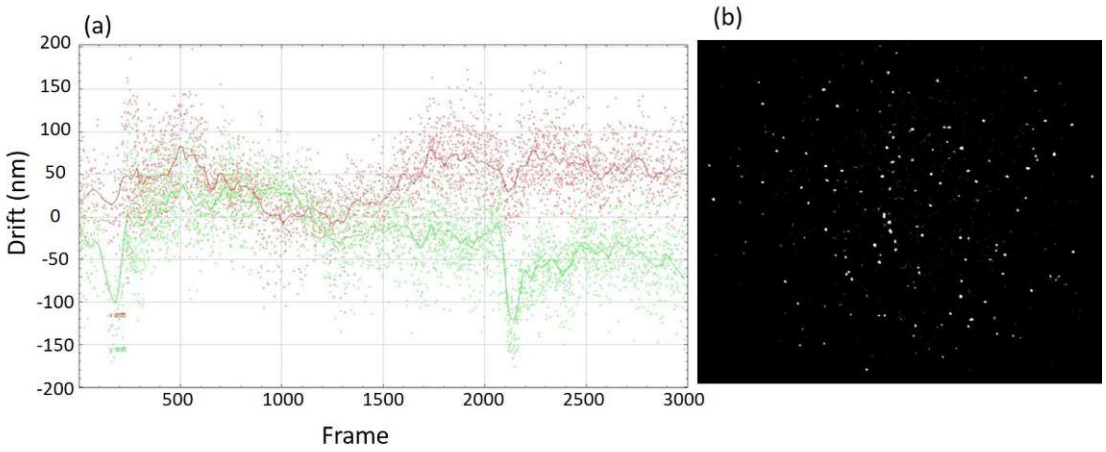

Figure 11: (a) Drift correction of AF 647 for 3000 frames at 110 K. The monitored drift in direction of x and y show in red and green respectively. Solid red and green lines are the applied drift correction. (b) Single molecule localization image of AF 647 at 110 K.

parameters such as photo bleaching, blinking in terms of ON and Off times of fluorophores and overall theoretical localization precision based on the total photon collection from one molecule. For simplicity, obtained histogram were plotted in the form of Box chart for comparison. Box-chart is using the 25 % (Q_1), middle and 75 % (Q_3) data value to characterize the distribution of the given data set as shown in Fig12. Additionally, the whisker is used to determine the outliers, where the position of whisker is usually define as 1.5 Interquartile range (IQR). Here, IQR is the difference between Q_1 and Q_3. Data value larger or smaller than the whiskers will be identified as outliers. In case the 1.5 IQR is exceeding the first/last data point in the set, the whisker is then defined by the first/last data point. Outliers are usually plotted as scatter points in the box-chart. In general, the smaller the box is, the higher precision the data set presents.

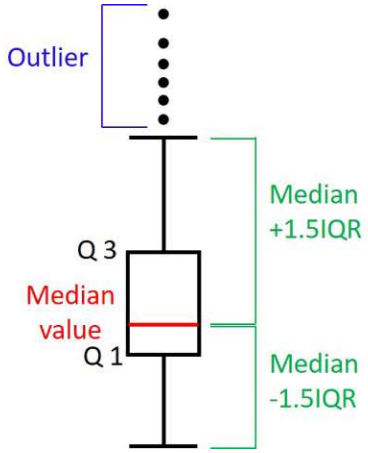

Figure 12: A example of box chart with Whiskers definition. Q1 (lower quartile) 25% of dataset, median value 50% value of dataset, Q3 (upper quartile) 75% value of dataset, IQR Interquartile range=Q3-Q1 the distance between the upper and lower quartiles. Outlier is median value pulse or minus 1.5 IQR range.

3 Results and Discussion

In this section, we will discuss the effect of cryogenic temperature on certain fluorescence properties of studied red fluorophores such as photostability in terms of photobleaching, photoblinking, On and Off times and overall theoretical localization precision which mainly depends on overall photon collection from single molecule. Further, we will also discuss about the effect of excitation power, exposure time and imaging interval on these parameters at cryogenic conditions. In the end, we will compare two studied fluorophores, AF 647 and Atto 647N (AT 647N) and determine the most suitable one for cryogenic application.

3.1 Photo-bleaching at cryogenic conditions

Photobleaching of fluorophores typically occurs either due to their chemical or physical interactions with the surrounding (e.g.interaction with oxygen, quenchers, protonation etc.) or via permanent physical transformation such as isomerization to other form or molecule disintegration. As all such process require physical motion of molecule; therefore, it can be minimized by freezing the sample to cryogenic temperatures. Here, we have tested a dried sample of AF 647 and Atto 647N dye on a glass coverslip (preparation discussed in method section) to examine and compare its photobleaching at normal (298K) and cryogenic (110K) temperatures. We used number of obtained localization in a frame as a parameter to define the change in the sample density (concentration) over time.

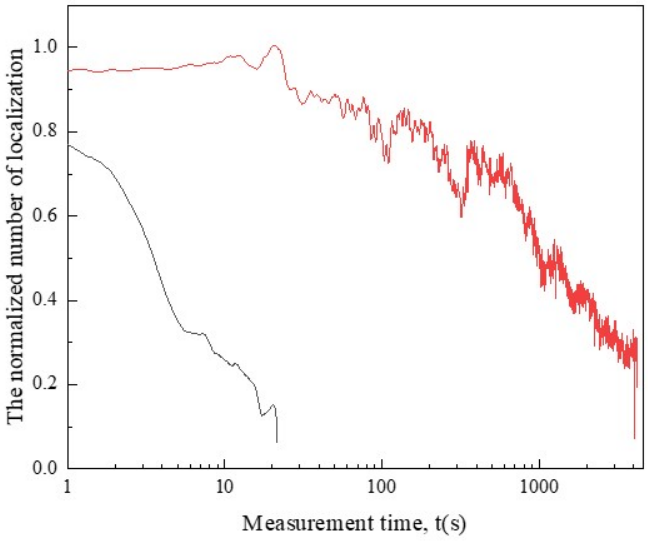

Figure 13: Photo-bleaching curves of Atto 647N at 298 K (black line) and 110 K (red) obtained with the same excitation parameters i.e. excitation laser power density of 0.2 kW/cm^2, exposure time 100 ms and interval of 10 ms.

Fig.13 represents the photobleaching curves of Atto 647N dye in room temperature (black) and at 110K(red), obtained at laser excitation power of 0.2 kW/cm^2 , 100 ms of continues exposure time and 10 ms of intervals between excitation pulses. As clear from graph, fluorophores at 298 K (Black Line) survive only 20-30 seconds, while the same dyes have slower photo-bleaching rate, and can actively emit fluorescence for more than 2000 seconds at 110 K. Thus, the half time of Atto 647N at 298 K and 110 K is measured around 5 seconds and 1000 seconds respectively i.e. almost 200 times higher. Therefore, from this we can easily conclude that organic dyes have definitely slower photo-bleaching rates and better photostability at cryogenic conditions.

3.2 Localization precision improvement

Benefiting from higher photostability and longer photon acquisition, we further analyzed the achievable localization precision in both individual and merged frames. We used our MATLAB code to count overall photons obtained from individual molecules. In particular, a clustering based algorithm is used in which obtained localizations within a circular region of 200 nm are considered as obtained from same molecule. But this algorithm strictly requires a nice separated single molecules by more then at least 200 nm distance. Therefore, only a well distributed single molecule sample can be used for such analysis.

Fig.14 (a) and (b) represents the distribution of collected photons from individual molecules of Atto 647N sample under cryogenic temperature (110 K) in single and merged frames respectively. Due to long time photostability of fluorophores at 110 K, we observed more than two hundred times increment in the overall photon collection from single molecules.

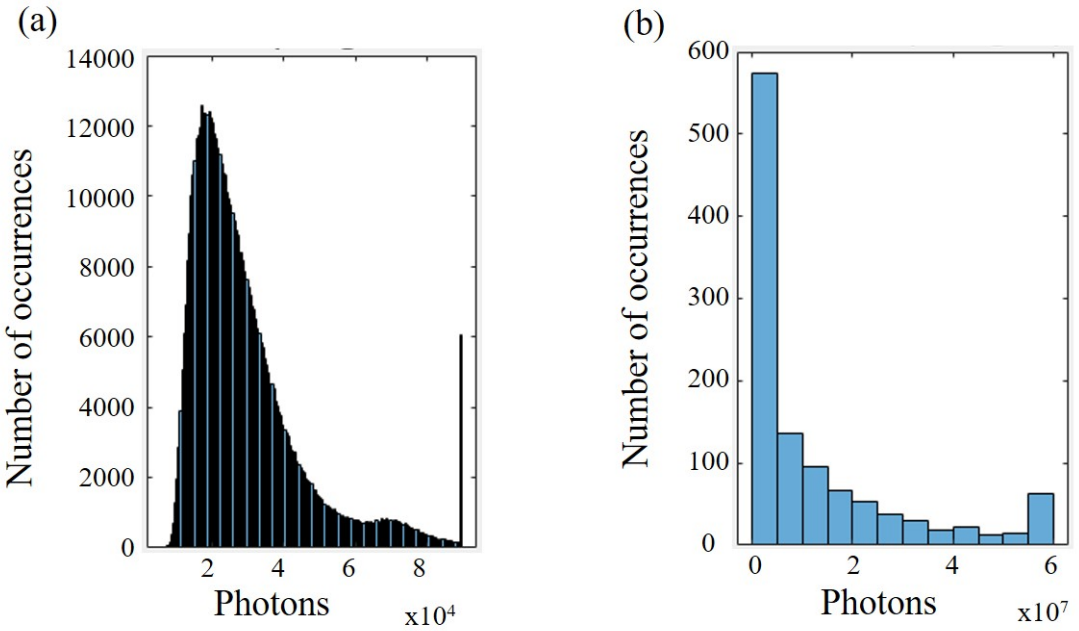

Figure 14: The number of photons of Atto 647N for 20000 frames with laser power density of 0.2 kW/cm^2, exposure time 100 ms and interval of 10 ms at 110 K. (a)The photo count of Atto 647N for single frame. (b) The photo count of Atto 647N for overall frame.

Based on the overall number of collected photons from single molecules in both individual and merged frames, one can determine the achievable localization precision using equation (5). Fig.15(a) and (b) represents the distribution of calculated localization precision of Atto 647N dye molecules at 110 K in single and merged frames respectively. Due to lesser photon count in single frame, we get the localization precision (LP) of around 10-30 nm with maximum occurrence of 20 nm. Whereas, in case of merged frame localization precision improves to the range of 0.1-5 nm with maxima around 0.6 nm. It should be noted that similar merging of frames to get more photon count per molecule can also be done for room temperature measurement.But, fast photobleaching at room temperature heavily limits even the overall photon collection, which leads to not very astonishing improvement in the localization precision as much we get at cryogenic conditions.

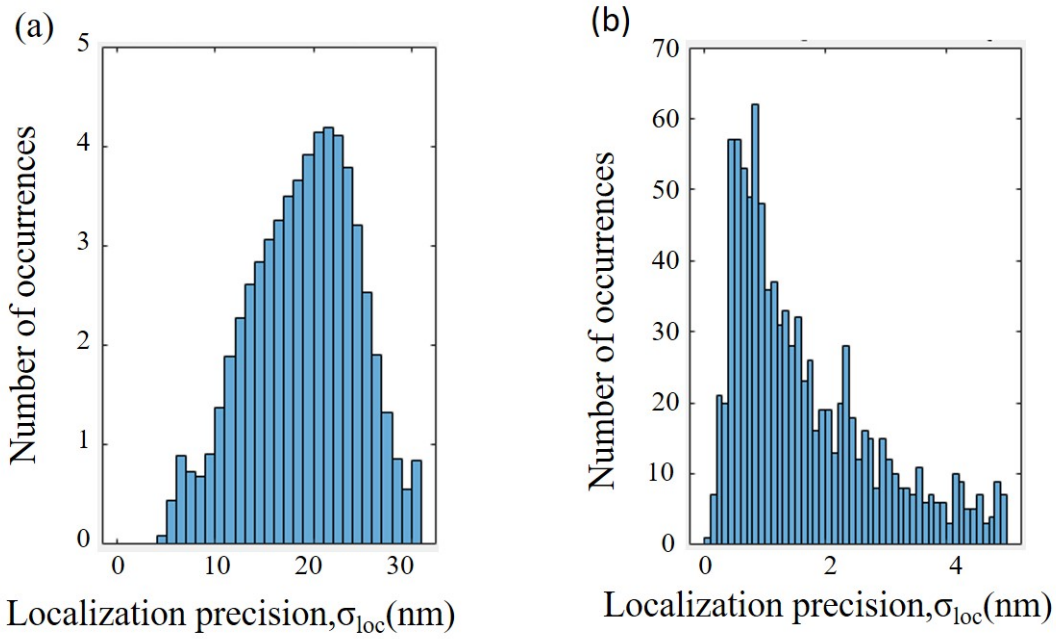

Figure 15: The calculated localization precision of Atto 647N for 20000 frames with laser power density of 0.2 kW/cm^2, exposure time 100 ms and interval of 10 ms at 110 K. (a) The localization precision for single frame. (b) The localization precision for overall frame.

3.3 Photo blinking properties: On times and Off times

As discussed before, beside localization precision, an efficient photoblinking of fluorophores possess equal contribution to define resolution capabilities of single molecule localization methods. In general, a molecule need to blink efficiently and should remain in Off state for significant time until other nearby molecules are imaged. Therefore, parameters such as On times and Off times are used to quantify the blinking efficiencies of fluorophores which eventually defines their high resolution capabilities. Fig. 16 represents observed On times and Off times of the same Atto 647N dye sample measured at 298 K (a,b) and 110 K (c,d). To calculate numerical values of On times, obtained histograms were fitted with following bi-exponential function as use of mono exponential function brings more error.

$$y = y_0 + A1 \exp(-x/\tau_1) + A2 \exp(-x/\tau_2) \tag{6}$$

This fitting equation shows two important parameters: a short (τ_1) and a long (τ_2) time-decay constant. The short and long time-decay constant τ show a superposition fitting by two individual exponential functions on the bar chart. The average value of time decay constant was further calculated by the following equation:

$$\tau_{avg} = \frac{A1 * \tau_1 + A2 * \tau_2}{A1 + A2} \tag{7}$$

From the observed increase in overall photon collection and improved localization precision at cryogenic conditions, we initially interpret that either increase in On times or decrease in Off times of fluorophore could be a possible reason behind this. However, in our analysis, the On times of Atto 647N dye was found to be almost unchangeable and stays around 30-40 ms for 0.2 kW/cm^2 excitation power, 100 ms exposure time and 10 ms of intervals (Fig. 16(a) and (c)). On the other hand, instead of decreasing, the Off times of Atto 647N at 110 K were estimated about four times higher than that of same sample measured at room temperature (Fig. 16(b) and (d)). Overall, we observed the Off times being nearly 6 and 27 times higher than that of the On times at 298 K and 110 K respectively.

The obtained very low Off times values at room temperature were mainly due to the use of dry sample for our measurements. Under normal room temperature SMLM experiments, various chemical such as STORM buffers are used to make additional long lived dark states of fluorophores which eventually not only enhances the photostability of fluorophore to certain extent but also increases its blinking efficiencies. But, as chemical induced blinking can not be used as an option in case of cryogenic experiments thus for an even comparison of the photo physics of dyes at 298 K and 110 K we need to use identical dry environment. So, from the observed changes in On and Off times of Atto 647N we can conclude that cryogenic temperatures stabilizes the natural dark state of fluorophore which is responsible for its efficient stochastic blinking. But, the Off times at 110 K are still not significantly higher for super resolution microscopy applications. Therefore, additional

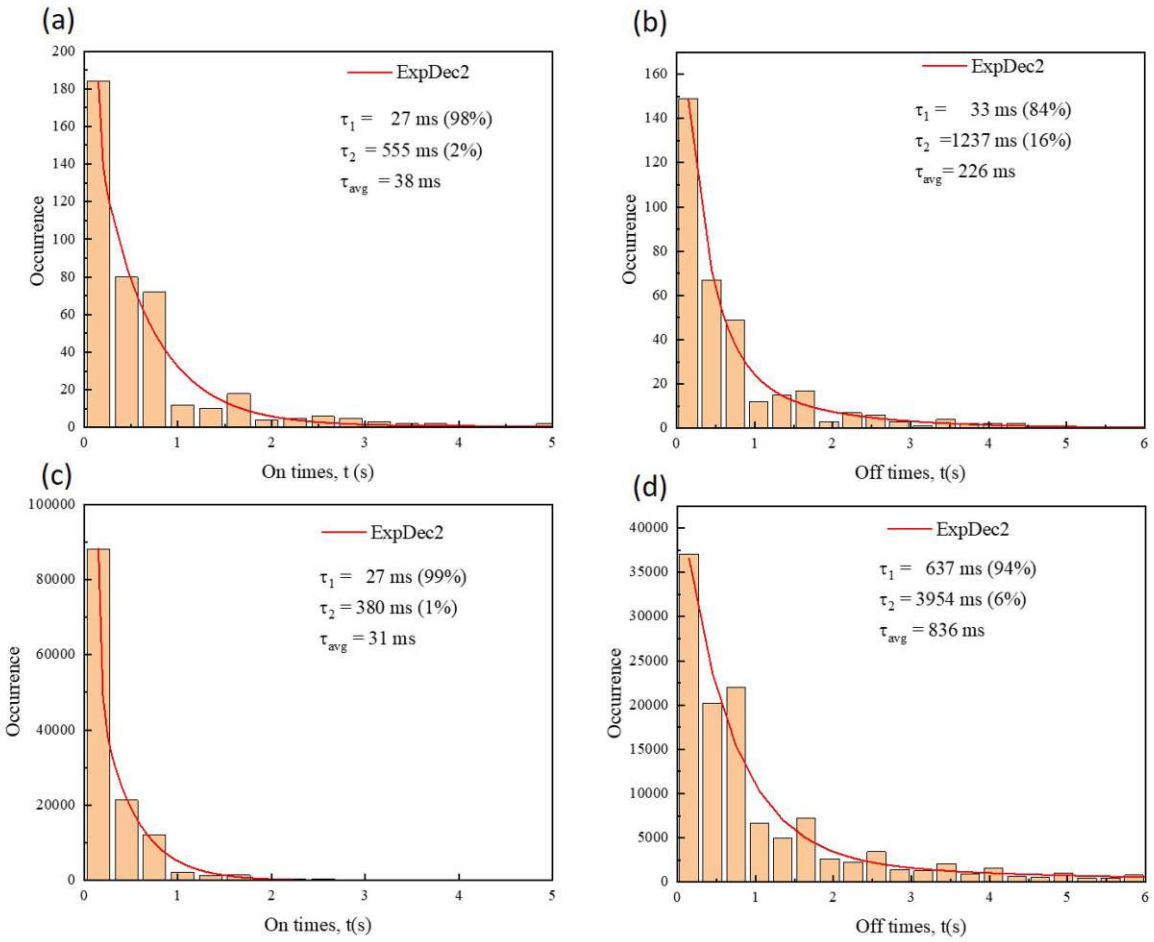

Figure 16: The On times and Off times of studied Atto 647N are fitted by bi-exponential function with excitation laser density 0.2 kW/cm^2, exposure time 100 ms and interval 10 ms at 298 K and 110 K. (a) On times of Atto 647N at 298 K. (b) Off times of Atto 647N at 298 K. (c) On times of Atto 647N at 110 K. (d) Off times of Atto 647N at 110 K.

methods for induced blinking such as selective polarized excitation, polarized emission filtering, multi color imaging etc may be additionally required to perform super resolution microscopy experiments at cryogenic temperatures.

3.4 Effect of excitation power

Benefiting from high photostability of fluorophores at cryogenic temperature, one can also use higher laser excitation power to accumulate high photons per frame. This can effectively reduces the measurement time for obtaining similar localization precision. However, very high laser powers can also have negative effects such as early bleaching of sample which leads to collection of less number of overall photons i.e. reduction in the overall localization precision. Therefore, a correct balance between excitation power and overall photon yield is prerequisite for attaining best possible localization precision at cryogenic conditions. So, we studied the influence of laser power on photobleaching of red dyes, AF 647 and Atto 647N at cryogenic temperature (110 K).

Fig. 17 shows change in normalized number of localizations with time (photobleaching) and distribution of localization precision of AF 647 dye at various excitation powers, recorded at 110 K for six minutes. An irradiation power of 0.1 kW/cm^2 to 1 kW/cm^2 was initially used for the experiment. We discarded the measurement made at 0.1 kW/cm^2 due to its very low signal to noise ratio. A clear trend of increasing photobleaching magnitude through the increasing of irradiated laser power was observed as shown in Fig. 17(a). Comparing the photobleaching curve at laser power density of 0.2 (black line) and 0.9 kW/cm^2 (green line), the half decay time (0.5 of normalized localization number) of AF 647 is around 260 and 30 seconds respectively, which is 8-9 times shorter when ramping the laser power density from 0.2 to 0.9 kW/cm^2. Therefore, we can conclude that excitation laser power density in this range has extremely strong effect on the photobleaching features of AF 647 dye.

In case of obtained overall localization precision (accumulated), AF 647 under the variation of excitation laser power density has similar results when they have the same imaging time as shown in Fig. 17 (b). The box chart of four distinct laser power shows their localization precision are in range of IQR = 5 nm (Q_1 = 2, Q_3 = 7 nm). The mean value of localization precision has slightly improved when laser intensity rises from 0.2 to 0.9 kW/cm^2, which is in range of 4-6 nanometer.

The calculated IQR of tested conditions are slightly showing a decreasing trend upon increasing the laser power density, where the IQR of 0.2 and 0.9 kW/cm^2 are 5 and 4 nm respectively. However, both the mean value and middle value (Q_2) of localization precision gives no significant change, indicating the measured power density range for the tested fluorophore gives no significant influence under this range of measuring time.

It is very interesting that even though the higher laser power density gives more significant photobleaching, the measured localization precision is however in the same value. This is likely due to the high photon counts that can be acquired under high power density within the first 100 s, which gives similar "total accumulated photon number" across different laser power densities within 350 s of measurement time. Therefore, we expect the difference should be revealed in experiment with longer duration, where the low laser power density set will give higher localization precision.

Further, Fig.18 shows photo-blinking cycle of AF 647 with varying excitation laser density of

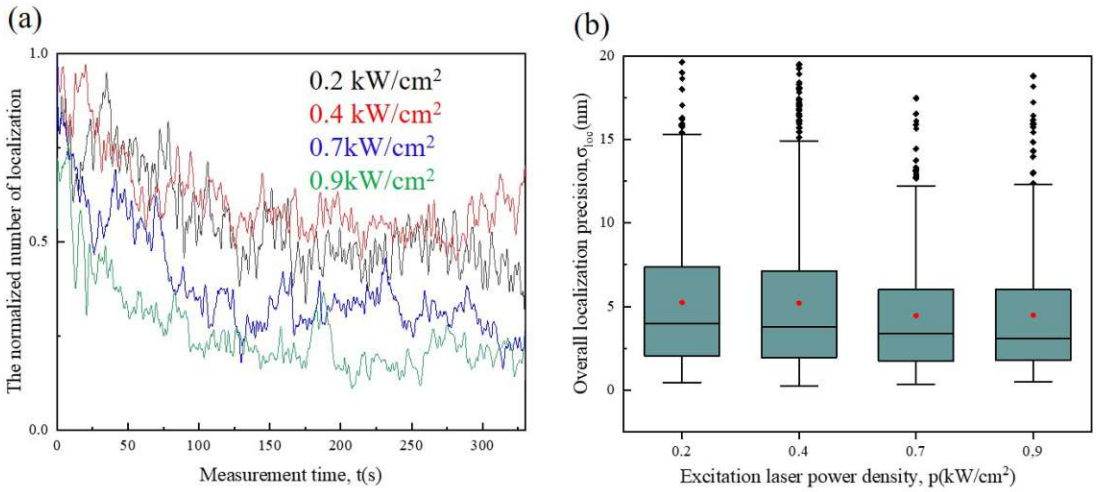

Figure 17: Excitation laser power dependent of AF 647 (a) photobleaching effect and (b) the calculated Localization Precision. The studied laser power density are 0.2, 0.4, 0.7 and 0.9 kW/cm^2 colored in black, red, blue and green respectively. Distribution of overall localization precision of the measured events are presented in form of box chart, where the lower box boundary, middle line and upper box boundary are Q_1 (25 %), middle value and Q_3 (75 %). The whisker displayed are with length of 1.5 times of IQR (Q_3 - Q_1), where the data points outside of the whisker are considered as outliers.

0.2, 0.4, 0.7 and 0.9 kW/cm^2 during a 350 seconds measuring time. In general, the lower laser power density is, the higher number of photo-blinking can be collected. The highest measured IQR of blinking feature of AF 647 is 50 at 0.2 kW/cm^2, where the IQR gradually reduces to around 20 when excitation laser power density is greater than 0.7 kW/cm^2. The trend of mean value of blinking feature is showing the same correlation as the IQR values over the power density change. It is around 40 number of photo-blinking cycle of AF 647 at 0.2 kW/cm^2, while the lowest mean value of photo-blinking number is 20 at 0.9 kW/cm^2.

Therefore, we can conclude that the photo-blinking properties of AF 647 highly depends on the excitation laser density. The higher excitation laser density we use, the higher photo-bleaching rate we observe. Hence, the lesser number of blinking can be detected.

The laser power dependency measurements of Atto 647N at 110K is shown in Fig.19 . During 350 seconds recording, the higher laser power density causes faster photobleaching. During relative short recording time, we can exclusively obtain the slightly difference of photo-bleaching effect. Short recording were made in order to complete all quantitative measurements with same sample on same day to avoid any sample uncertainty. Fig19 (b) represents the variation in overall localization precision of Atto 647N at 110 K with respect to laser power density. Here, the box chart shows the shortest range of localization precision within Q_1 to Q_3 and the highest mean (2.5 nm) and median value (1.5 nm) of localization precision recorded at 0.2 kW/cm^2. On the other hand, the higher excitation power of 0.4 and 0.7 kW/cm^2 have higher photo-bleaching rate and lower photo-blinking events on Atto 647N, that leads to poor mean value and larger value of Q_1-Q_3 of localization precision. The value of Q_1-Q_3 of localization precision at 0.2 kW/cm^2 of

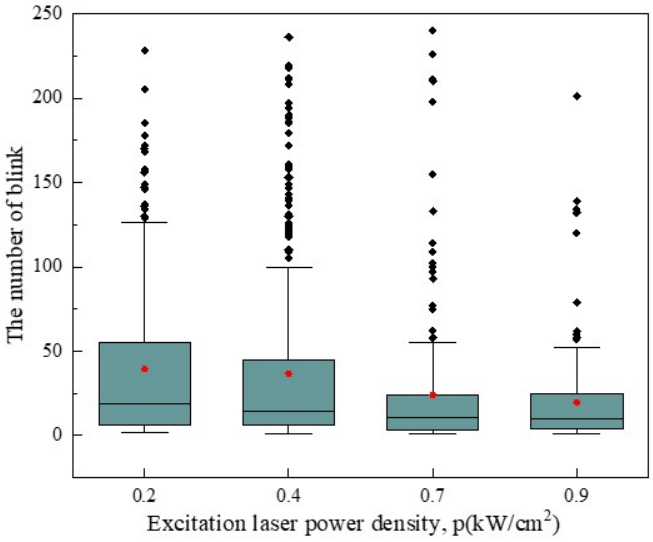

Figure 18: The photo-blinking events of AF 647 under variation of excitation laser power density for 350 seconds of recording with 100ms exposure time and 10ms interval.

laser density irradiation is 1-2.5 nm; however, the overall localization precision within Q_1-Q_3 has broader range (1-6 nm) at 0.4 and 0.7 kW/cm^2 laser irradiation. Therefore, excitation power of 0.2 kW/cm^2 provides best localization precision for AT647N.

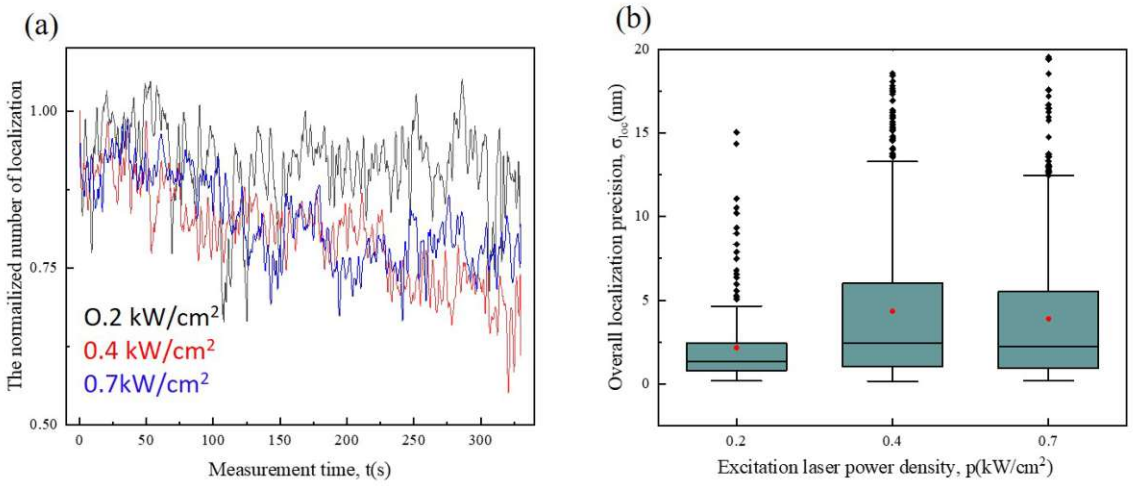

Figure 19: Excitation power dependent (a) photobleaching effect and the calculated (b) Localization Precision of Atto 647N dye.

3.5 Effect of exposure time

The other important parameter which can also increase the single frame photon yield is exposure time. However, a longer exposure time can also lead to faster photobleaching of fluorescent dyes. Additionally, any vibrational drift in the sample during long exposure time can also increase the standard deviation of diffraction limited spot which also directly influence the localization precision. Therefore, we examined an effect of exposure time on the photobleaching behaviour of red fluorescent dyes and their achievable localization precision with our setup. Fig.20 shows the photo-bleaching curve and localization precision of AF 647 with variation of excitation exposure time from 100 to 400ms, recorded at excitation power of 0.2 kW/cm^2 and 10 ms interval time. Here, we do not clearly see any significant effect of photobleaching with increasing the exposure times. It is somehow strange to interpret since we expected higher photobleaching rates at longer exposure time. But, this may not be valid in the range of studied exposure times, since the data is relatively noisy where only a time range from 200 - 400 s shows clear difference. But unexpectedly, even there we observed increase in the number of active fluorophores at higher exposure time of 400 ms. This could possibility due to long time excitation/observation of fluorophores at high exposure times which helps detecting certain localizations which are undetectable with smaller exposure times.

Next, the overall localization precision found varying with change in excitation exposure time as shown in Fig. 20(b), As mentioned before, localization precision depends on two factors i.e. 1) the number of detected photons and 2) the FWHM of obtained point spread function(PSF). With increase in excitation exposure time, more emitted photon can be collected, which results in smaller (Improved) values of localization precision. However, higher exposure time can also broader fluorescent signals due to sample drifts/vibrations during photon collection of single frame, which results in the higher FWHM of PSF. This leads to the larger value of localization precision. Thus, both factors combine to make the final calculated localization precision value fluctuating. Therefore, it is hard to conclude if the studied range of exposure time gives a clear impact on the photobleaching effect and localization precision of AF 647.

Then we studied the effect of exposure time on Atto 647N. Fig.21(a) and (b) indicates the photo-bleaching effect and the overall localization precision of Atto 647N with variation of excitation exposure time at 110 K respectively. These three photo-bleaching curve recorded at 100, 200 and 400 ms exposure time shows similar trend during 1200 seconds of measurements with slight fluctuations caused by sample de-focusing during measurement. However, from the variation in overall localization precision i.e. figure 21 (b), we fund that the higher localization precision can be obtain by 50 and 100 ms exposure time with the mean value of 3 and 2.5 nm respectively. But, the mean value of higher 200 and 400 ms exposure time are around 6 nm. Thus 200 and 400 ms of exposure time shows larger IQR (5-6 nm) while the 50 and 100 ms exposure time shows shorter IQR (2 nm) in localization precision. Therefore, variation of exposure time does not cause obvious difference on photo-bleaching curve for Atto 647N like AF 647, but shorter exposure

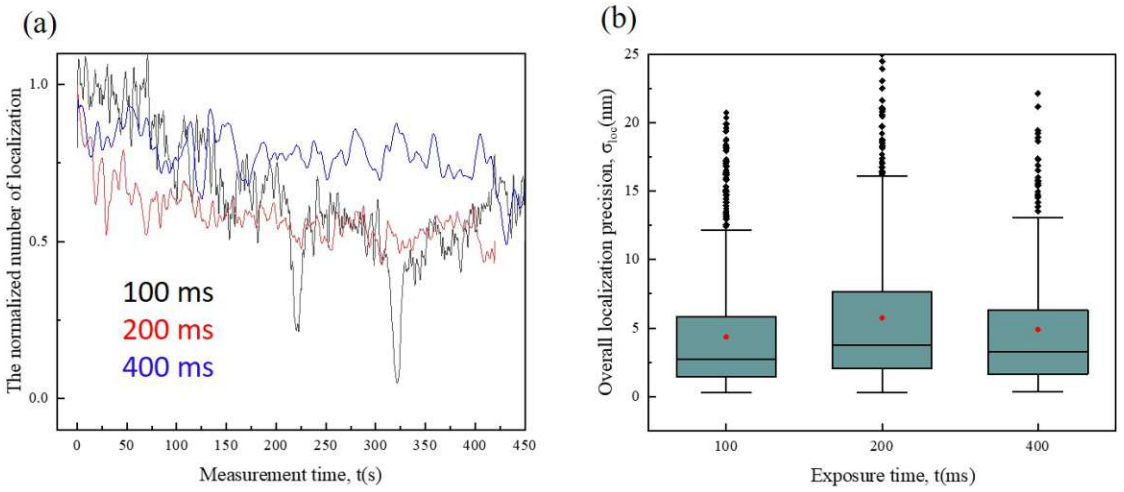

Figure 20: Influence of exposure time dependent photobleaching and calculated localization precision of dye AF 647. (a) Normalized number of localization change compared with three studied exposure time of 100 (black), 200 (red) and 400 ms (blue) respectively, over 450 s of measurement time. (b) Resulting localization precision under different laser exposure time.

time causes better overall localization precision of Atto 647N due to smaller standard deviations in obtained PSF. Overall, the best localization precision for AT647 could be reached by 100 ms excitation exposure time during these four distinct exposure time.

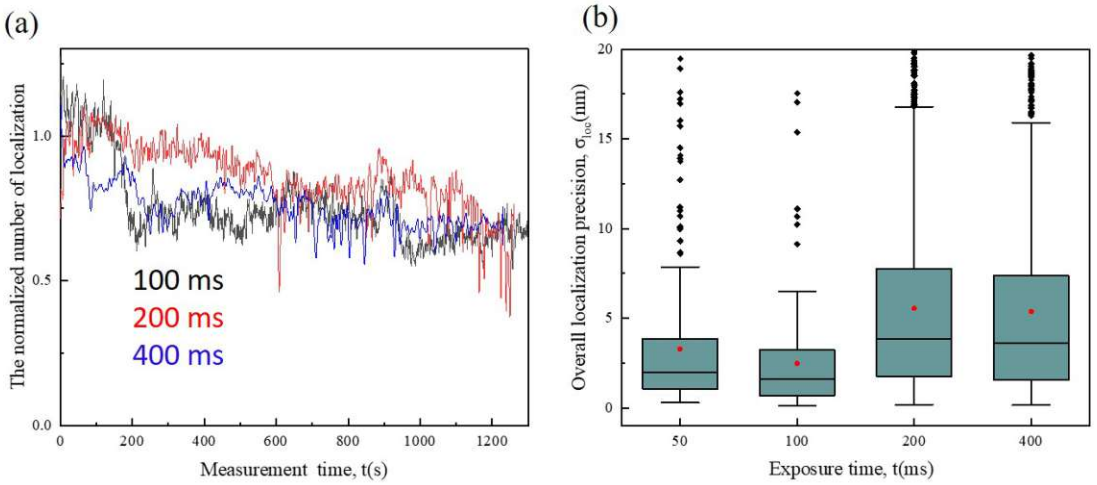

Figure 21: Excitation exposure time dependent of studied dye Atto 647N (a) photobleaching effect and (b)the calculated Localization Precision. The studied laser exposure time are 100, 200 and 400 ms colored in black, red and blue respectively. Distribution of localization precision of the measured events are presented in form of box chart, where the lower box boundary, middle line and upper box boundary are Q_1 (25 %), middle value and Q_3 (75 %). The whisker displayed are with length of 1.5 times of IQR (Q_3 - Q_1), where the data points outside of the whisker are considered as outliers.

3.6 Effect of excitation intervals

Intervals between excitation pulses plays an important role to reduce fast photobleaching of dyes by providing sufficient times to dye molecule for relaxation from dark states. But it also increases the data acquisition time leading to the possibility of more sample drift per measurement. In this context, we studied the effect of imaging interval on photo physical properties of Atto 647N at 110 K as shown in Fig.22. The three bleaching curve for Atto 647N in Fig.22 (a) corresponds to 10 ms (black), 100 ms (red) and 200 ms (blue) pulse interval in which we didn't see very significant difference. However after 5000 frame (1000s of total exposure time), the photo-bleaching curve for 10 ms interval shows a little more bleaching as compared to other curves. This indicates more bleaching rate for shorter interval time. This may be either due to expected insufficient time for dye relaxation or due to local heating of the sample.

Further, Fig.22 (b) shows overall localization precision obtained from same data set of Atto 647N for three different pulse interval. The IQRs of overall localization precision of measured systems are around 2-3 nm, where the 10 ms interval has smallest IQR, indicating better data precision. Additionally, 10 ms interval has lowest mean value and median value of localization precision of 2.5 and 1.0 nm respectively. The mean value of localization precision is slightly larger than its median value, which is due to the contribution of outliers with larger values. We observed similar interval dependency measurements of AF 647 at 110 K. Overall, best values for localization precision were found when 10 ms interval is used.

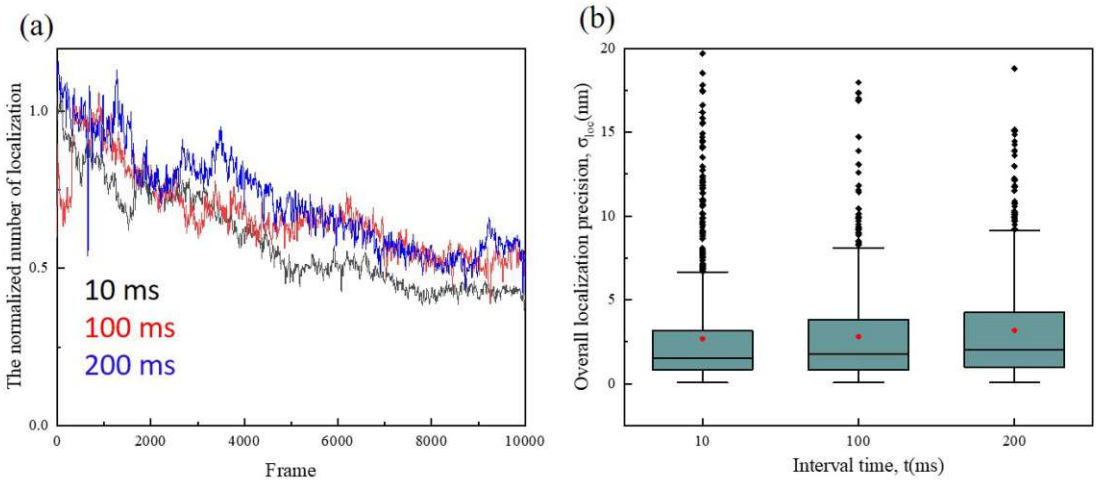

Figure 22: Influence of laser pulse interval dependent photobleaching and calculated localization precision of dye Atto 647N. (a) Normalized number of localization change compared with three studied irradiation interval time of 10 (black), 100 (red) and 200 ms (blue) respectively, over 11000 frame of measurement. (b) Resulting localization precision under different irradiation interval time.

3.7 Comparison between Atto 647N and Alexa fluor 647 dye

Lastly, we compared all results obtained from Alexa fluor 647 and Atto 647N dye in order to determine most suitable fluorophore among them for cryo fluorescence microscopy application. Same dry samples of both dyes were analysed at 110 K using same excitation parameters i.e. excitation laser density of 0.2 kW/cm^2, 100 ms exposure time and 10 ms pulse intervals. Results obtained for On and Off times are shown in Fig. 23 and 24. The obtained histograms for On and Off times of both studied dyes are fitted by a bi-exponential function with a short τ_1 and a long time-decay constant τ_2 (see details discussion in section 3.3 On times and Off times). Here, we focus our discussion on the decay profile of majority population, i.e. short time-decay constant τ_1 of On times and Off times of fluorophores. The τ_1 of On times of both studies dyes have similar value around 25 ms. However, the τ_1 of Off times of AF 647 and Atto 647N were measured as 850 and 637 ms respectively, which is 34 and 24 times longer than its On times duration respectively. The calculated average time-decay constant τ_{avg} for Off times of AF 647N is observed around 1110 ms, which is 274 ms higher than the τ_{avg} for Off times of Atto 647N, which is 836 ms. So overall, both dyes possess similar average On times but AF 647 has slightly larger Off times then AT647N, which makes it a little more preferable for SMLM methods.

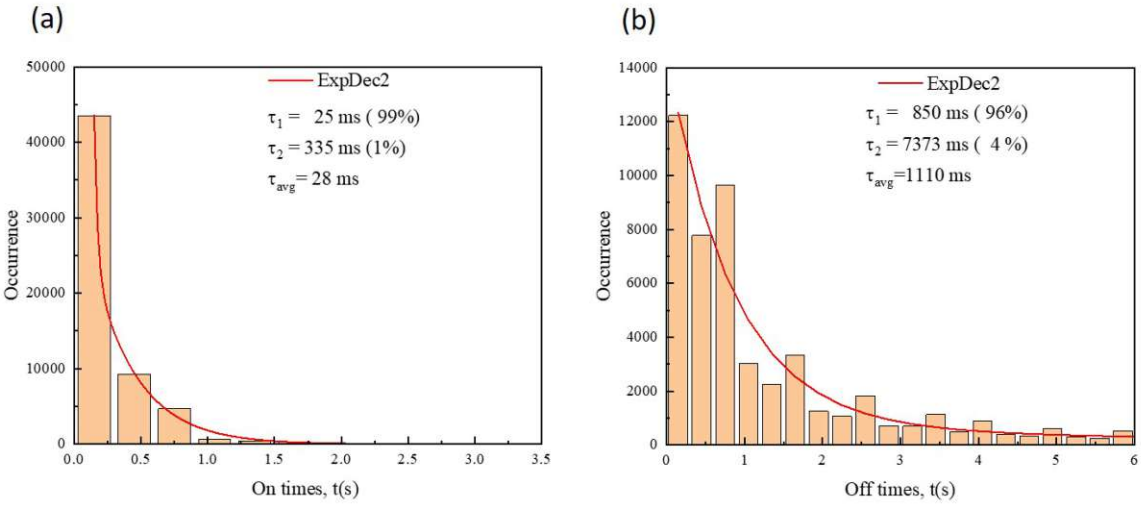

Figure 23: On and Off times of studied dye AF 647 are fitted by bi-exponential function at excitation laser density 0.2 kW/cm^2, exposure time 100 ms and interval 10 ms at 110 K.

Next, we compared the photobleaching behaviour of these dyes at normal and cryogenic temperature. Both organic dye samples remains active for more than 2000 seconds at 110 K, which is around 100 times more as compared to observed 20 s of active time at room temperature. This confirms that AF 647 and Atto 647N have relatively slower photo-bleaching rate (better photostability) at cryogenic temperature. Additionally, under cryogenic condition, the half time of AF 647 and Atto 647N were found to be around 290 and 1050 seconds respectively, as shown in Fig25 (a). This means that Atto 647N has better i.e. nearly four times higher photostability at

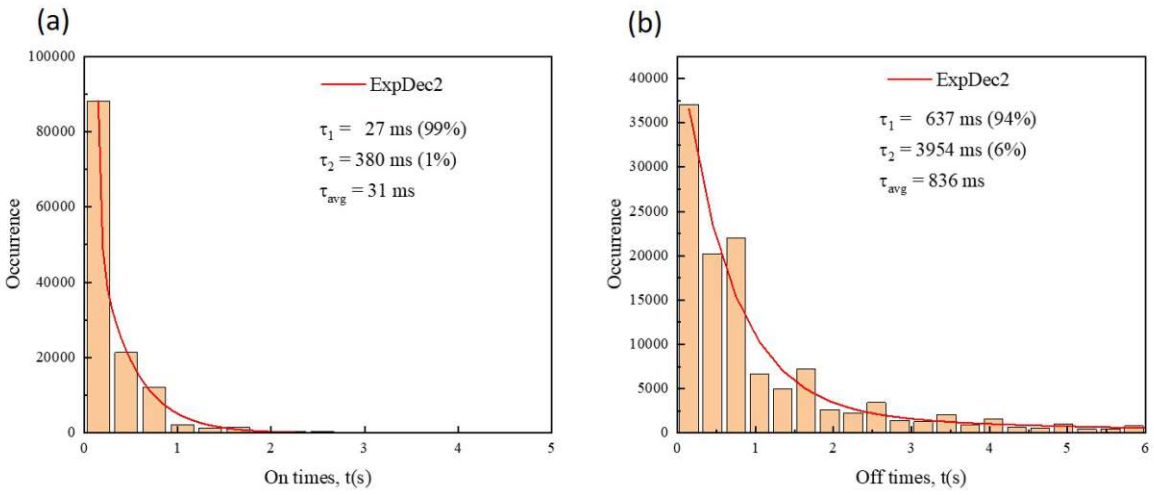

Figure 24: On and Off times of studied dye Atto 647N with bi-exponential fitting at excitation laser density 0.2 kW/cm^2, exposure time 100 ms and interval 10 ms at 110 K.

cryogenic temperature than AF 647.

Next, we compared the brightness of these two dyes in terms of photon counts per molecule per frame, analysed from the same experimental data. The box chart in Fig.25(c) shows of both organic dyes have similar Q_1-Q_3 values and mean value of photo count which is from 1x10^4 to 5x10^4 photons and around 3x10^4 photons respectively per frame at 298 K. If we look at two dyes on cryogenic condition, Q_1-Q_3 of photons count indicates shorter range compared to room temperature and Atto 674N has slightly higher mean value of photons number 3x10^4 than the mean value of AF 647 photons number 3x10^4. However, the overall photon number at 110 K has significant growth compared to 298 K as shown in Fig 25 (d). The overall photons count of Atto 647N has higher mean value (1.5x10^7) than AF 647 with 3x10^6 at 110 K. The mean value of photons number of Atto 647N and AF 647 are approximately 6.5x10^5 and 2x10^5 at 298 K respectively, and Atto 647N and AF 647 have 23 and 15 times increases on the mean value of photon count.

In terms of overall localization precision, Atto 647N and AF 647 at 110 K can reach higher localization precision values than at 298 K as shown in Fig25 (b). The median value of overall localization precision of Atto 647N at 110 K can achieve 1-2 nm whereas at 298 K, it is 6-7 nm. AF 647 can reach 2-3 nm of median value of localization precision at 110 K. In contrast, 8-9 nm of median value overall localization precision can be obtained at 298 K.

Further, we also compared the blinking events of both dyes at normal and cryogenic conditions. Fig.26 indicates the significant difference of photo-blinking number between 298 K and 110 K for both studied dyes Atto 647N and AF 647. Generally speaking, the number of blinking events for both organic dyes at 110 K have larger IQR value and mean values than at 298 K. The IQR values of blinking number of both fluorophores are approximately 200 at 110 K, however, there is around 8 for IQR values of blinking number of both dyes. This is mainly due to the possibility of long time measurements in case of cryogenic conditions, which report more blinking events of dyes.

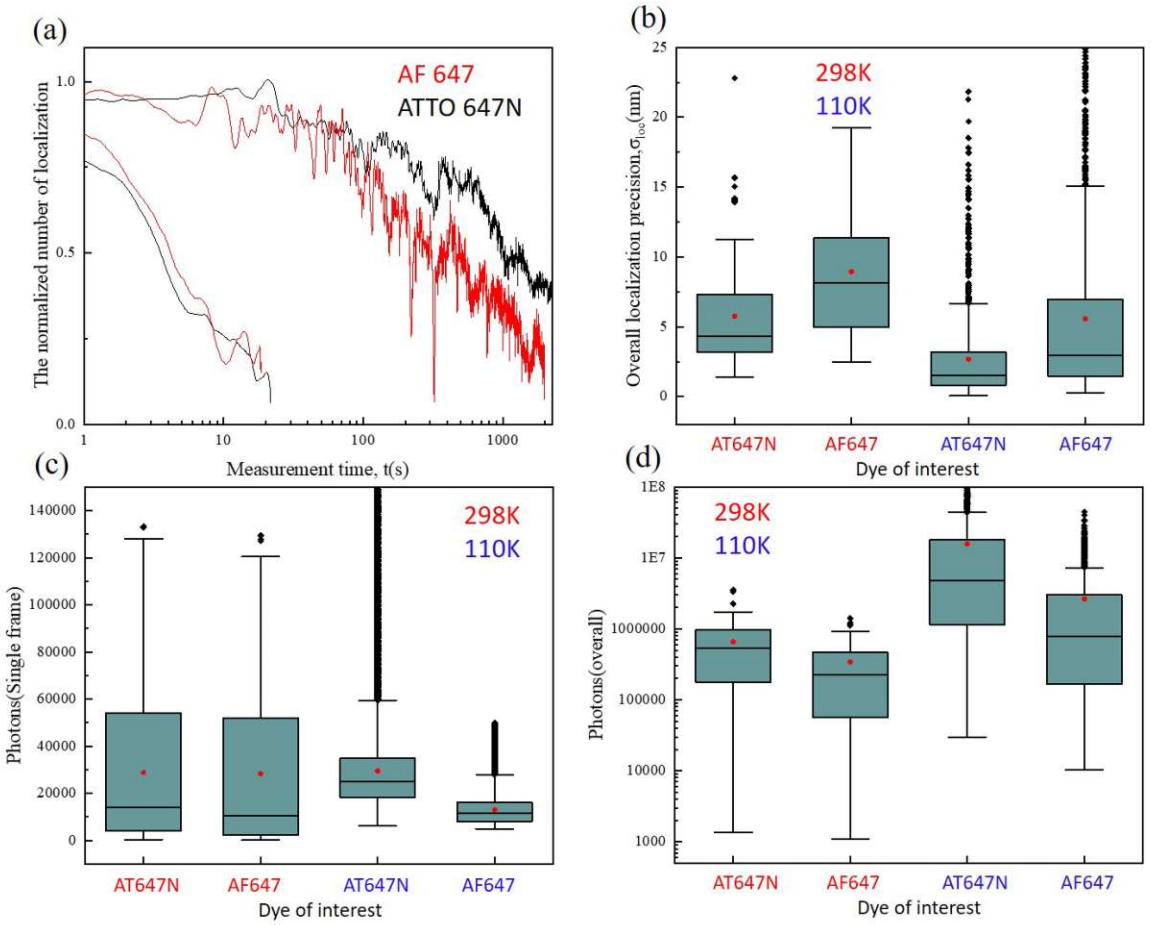

Figure 25: Comparison of AF 647 and Atto 647N at 298 K and 110 K. (a) The photobleaching effect of AF 647(red line) and Atto 647N at 298K and 110 k, and both organic dyes are recording for longer time at 110 K. (b) The overall localization of AF 647 and Atto 647N at 298 K (red label) and 110 K (blue label). (c) The photons count of single frame of AF 647 and Atto 647N at 298 k(red) and 110 K (blue). (d) The total photons number of AF 647 and Atto 647N at 298 K (red) and 110 K (blue).

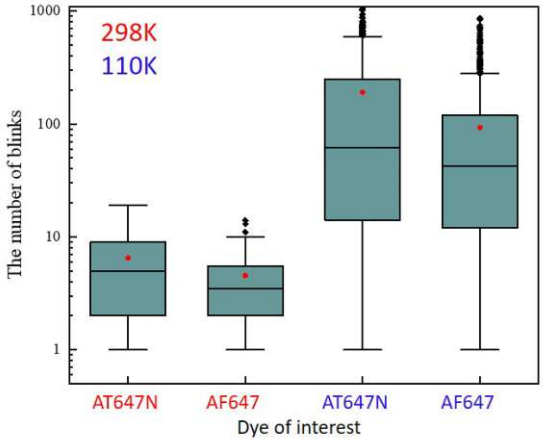

Figure 26: Comparison of the number of photoblinkng of AF 647 and Atto 647N at 298 K(red) and 110 K(blue).

4 Conclusions

Based on the results presented in this thesis, we can simply conclude that cryogenic conditions very effectively enhances the photostability of fluorophores allowing collection of very high number of photons from single molecules. This eventually leads to dramatic increase in localization precision below one nanometer.

Furthermore, cryogenic conditions enhances the standard Off times of fluorophore to some extent but not significantly higher. Therefore, additional induced blinking methods such as selective polarized excitation of fluorophores, polarization filtering of fluorescence signal or multi color imaging are proffered to be used in cryo super resolution microscopy experiments.

The photon count of fluorescent signals at initial stage can be significantly increased, when increasing the laser power density. Also, certain high laser power density make the photon count of fluorescent signals reach a plateau close to certain value (better signal to noise ratio). It means the measured photon number of a given localization is not proportional to the laser power density at certain range, but depends on what kind of dye we used. Although the higher excitation laser power density provide higher photon counts in the studied dyes, but it also causes faster photobleaching rate. It is therefore important to carefully choose the laser power density based on the system and time frame of study. In our experiments, we observed laser power of 0.2 kW/cm^2 ideal for getting acceptable signal to noise ratio with minimum photobleaching rates.

Variation of exposure time from 50 to 400 ms does not impact significantly on photobleaching properties of studied dyes within 20 minutes of recording time. However, it brings increase in the standard deviation of imaged diffraction limited spot (PSF) which leads to increase in localization uncertainties. Therefore, we prefer to use minimum exposure time which can provide acceptable signal to noise ratio. In our case, it was 100 ms of exposure time.

Increase in the pulse interval was also found ineffective on photobleaching rates of both studied dyes. Thus we preferred to stick with 10 ms of intervals. Continues exposure is avoided due to its possibility for local heating of the sample.

Finally, on comparing Alexa fluor 647 and Atto 647 N, we found Atto 647N more photo-stable and brighter than AF 647. This results in better localization precision (below 1 nm) in case of Atto 647N. Thus, Atto 647N is definitely preferred over AF 647 for high resolution microscopy. But it should be noted that, the Off times for Atto 647N were found little smaller then AF 647. However, these values are still not sufficient enough for high resolution microscopy of complex structures. Therefore, additional induced blinking methods are preferable in case of both dyes.

Abbreviations and Symbols

Abbreviations	Description
AF 647	Alexa Fluor 647
AT 647N	Atto 647N
BS	Beam Splitter
CF	Cleanup Filter
FWHM	Full Width at Half Maximum
HOMO	the Highest Occupied Molecular Orbital
IC	Internal Conversion
IQR	Interquartile Range
LUMO	the Lowest Unoccupied Molecular Orbital
M	Mirror
NA	Numerical Aperture of Objective Lens
PSF	Point Spread Function
PBS	Phosphate Buffered Saline
Q_1	First Quartile
Q_3	Third Quartile
sCMOS	scientific Complementary Metal Oxide Semiconductor
SMLM	Single-Molecular Localization Microscopy
WP	Wave Plate

Symbols	Description
n	Refractive Index of the Medium
θ	Half Angular Aperture of the objective lens
D	Minimum Resolvable Distance
E	Energy of Electronic Transition
h	Planck Constant
c	Speed of light
λ	Wavelength
A	Absorbance of a substance
ε	Molar Absorption Coefficient of a Material
$[c]$	Molar Concentration of Material
d	the Distance of Optical Path Length
$\sigma_{\mathbf{loc}}$	Localization Precision
$\sigma_{\mathbf{psf}}$	Full Width at Half Maximum (FWHM) of Point Spread Function (PSF)
N	Count of Collected Photos
τ	Time Decay Constant

5 References

References

[1] Mayeul Collot, Tkhe Kyong Fam, Pichandi Ashokkumar, Orestis Faklaris, Thierry Galli, Lydia Danglot, and Andrey S Klymchenko. Ultrabright and fluorogenic probes for multicolor imaging and tracking of lipid droplets in cells and tissues. *Journal of the American Chemical Society*, 140(16):5401–5411, 2018.

[2] Mika Rämet, Pascal Manfruelli, Alan Pearson, Bernard Mathey-Prevot, and R Alan B Ezekowitz. Functional genomic analysis of phagocytosis and identification of a drosophila receptor for e. coli. *Nature*, 416(6881):644–648, 2002.

[3] Alexandra Aicher, Winfried Brenner, Maaz Zuhayra, Cornel Badorff, Schirin Massoudi, Birgit Assmus, Thomas Eckey, Eberhard Henze, Andreas M Zeiher, and Stefanie Dimmeler. Assessment of the tissue distribution of transplanted human endothelial progenitor cells by radioactive labeling. *Circulation*, 107(16):2134–2139, 2003.

[4] Brian Herman. *Fluorescence microscopy*. Garland Science, 2020.

[5] HJ Tanke, J Wiegant, RPM Van Gijlswijk, V Bezrookove, H Pattenier, RJ Heetebrij, EG Talman, AK Raap, and J Vrolijk. New strategy for multi-colour fluorescence in situ hybridisation: Cobra: Combined binary ratio labelling. *European Journal of Human Genetics*, 7(1):2–11, 1999.

[6] Ben NG Giepmans, Stephen R Adams, Mark H Ellisman, and Roger Y Tsien. The fluorescent toolbox for assessing protein location and function. *science*, 312(5771):217–224, 2006.

[7] Monpichar Srisa-Art, Emily C Dyson, Andrew J deMello, and Joshua B Edel. Monitoring of real-time streptavidin- biotin binding kinetics using droplet microfluidics. *Analytical chemistry*, 80(18):7063–7067, 2008.

[8] Igor L Medintz and Niko Hildebrandt. *FRET-Förster resonance energy transfer: from theory to applications*. John Wiley & Sons, 2013.

[9] Kenji AK Tanaka, Kenichi GN Suzuki, Yuki M Shirai, Shusaku T Shibutani, Manami SH Miyahara, Hisae Tsuboi, Miyako Yahara, Akihiko Yoshimura, Satyajit Mayor, Takahiro K Fujiwara, et al. Membrane molecules mobile even after chemical fixation. *Nature methods*, 7 (11):865–866, 2010.

[10] HB Currier and Siegfried Strugger. Aniline blue and fluorescence microscopy of callose in bulb scales ofallium cepa l. *Protoplasma*, 45(4):552–559, 1956.

[11] Cindi L Schwartz, Vasily I Sarbash, Fazoil I Ataullakhanov, J Richard Mcintosh, and Daniela Nicastro. Cryo-fluorescence microscopy facilitates correlations between light and cryo-

electron microscopy and reduces the rate of photobleaching. *Journal of microscopy*, 227(2): 98–109, 2007.

[12] Susan J Nixon, Richard I Webb, Matthias Floetenmeyer, Nicole Schieber, Harriet P Lo, and Robert G Parton. A single method for cryofixation and correlative light, electron microscopy and tomography of zebrafish embryos. *Traffic*, 10(2):131–136, 2009.

[13] Felipe Moser, Vojtěch Pražák, Valerie Mordhorst, Débora M Andrade, Lindsay A Baker, Christoph Hagen, Kay Grünewald, and Rainer Kaufmann. Cryo-sofi enabling low-dose super-resolution correlative light and electron cryo-microscopy. *Proceedings of the National Academy of Sciences*, 116(11):4804–4809, 2019.

[14] David P Hoffman, Gleb Shtengel, C Shan Xu, Kirby R Campbell, Melanie Freeman, Lei Wang, Daniel E Milkie, H Amalia Pasolli, Nirmala Iyer, John A Bogovic, et al. Correlative three-dimensional super-resolution and block-face electron microscopy of whole vitreously frozen cells. *Science*, 367(6475), 2020.

[15] Catherine G Galbraith and James A Galbraith. Super-resolution microscopy at a glance. *Journal of cell science*, 124(10):1607–1611, 2011.

[16] Martin Ovesnỳ, Pavel Křížek, Josef Borkovec, Zdeněk Švindrych, and Guy M Hagen. Thunderstorm: a comprehensive imagej plug-in for palm and storm data analysis and super-resolution imaging. *Bioinformatics*, 30(16):2389–2390, 2014.

[17] Markus Sauer, Johan Hofkens, and Jörg Enderlein. *Handbook of fluorescence spectroscopy and imaging: from ensemble to single molecules*. John Wiley & Sons, 2010.

[18] Nicolas Renier, Zhuhao Wu, David J Simon, Jing Yang, Pablo Ariel, and Marc Tessier-Lavigne. idisco: a simple, rapid method to immunolabel large tissue samples for volume imaging. *Cell*, 159(4):896–910, 2014.

[19] Leila Nahidiazar, Alexandra V Agronskaia, Jorrit Broertjes, Bram van den Broek, and Kees Jalink. Optimizing imaging conditions for demanding multi-color super resolution localization microscopy. *PLoS One*, 11(7):e0158884, 2016.

[20] Shin-nosuke Uno, Mako Kamiya, Toshitada Yoshihara, Ko Sugawara, Kohki Okabe, Mehmet C Tarhan, Hiroyuki Fujita, Takashi Funatsu, Yasushi Okada, Seiji Tobita, et al. A spontaneously blinking fluorophore based on intramolecular spirocyclization for live-cell super-resolution imaging. *Nature chemistry*, 6(8):681–689, 2014.

[21] Stokes shift. URL `https://en.wikipedia.org/wiki/Stokes_shift`.

[22] Daniel Böning, Franz-Ferdinand Wieser, and Vahid Sandoghdar. Polarization-encoded colocalization microscopy at cryogenic temperatures. *ACS Photonics*, 2020.

[23] Markus Sauer and Mike Heilemann. Localization-based super-resolution microscopy. *Fluorescence Microscopy: From Principles to Biological Applications*, 2017.

[24] Fluorescence microscope. URL `https://en.wikipedia.org/wiki/Fluorescence_microscope`.

[25] Harald Volkmann. Ernst abbe and his work. *Applied Optics*, 5(11):1720–1731, 1966.

[26] Airy disk. URL `https://en.wikipedia.org/wiki/Airy_disk`.

[27] The rayleigh criterion. URL `http://hyperphysics.phy-astr.gsu.edu/hbase/phyopt/Raylei.html`.

[28] Stefan W Hell and Jan Wichmann. Breaking the diffraction resolution limit by stimulated emission: stimulated-emission-depletion fluorescence microscopy. *Optics letters*, 19(11):780–782, 1994.

[29] Mats GL Gustafsson. Surpassing the lateral resolution limit by a factor of two using structured illumination microscopy. *Journal of microscopy*, 198(2):82–87, 2000.

[30] Eric Betzig, George H Patterson, Rachid Sougrat, O Wolf Lindwasser, Scott Olenych, Juan S Bonifacino, Michael W Davidson, Jennifer Lippincott-Schwartz, and Harald F Hess. Imaging intracellular fluorescent proteins at nanometer resolution. *Science*, 313(5793):1642–1645, 2006.

[31] Michael J Rust, Mark Bates, and Xiaowei Zhuang. Sub-diffraction-limit imaging by stochastic optical reconstruction microscopy (storm). *Nature methods*, 3(10):793–796, 2006.

[32] Honglin Li and Joshua C Vaughan. Switchable fluorophores for single-molecule localization microscopy. *Chemical reviews*, 118(18):9412–9454, 2018.

[33] Markus Sauer and Mike Heilemann. Single-molecule localization microscopy in eukaryotes. *Chemical reviews*, 117(11):7478–7509, 2017.

[34] Christiaan N Hulleman, Weixing Li, Ingo Gregor, Bernd Rieger, and Jörg Enderlein. Photon yield enhancement of red fluorophores at cryogenic temperatures. *ChemPhysChem*, 19(14):1774–1780, 2018. URL `https://chemistry-europe.onlinelibrary.wiley.com/doi/abs/10.1002/cphc.201800131`.

[35] Lin Wang, Benji Bateman, Laura C Zanetti-Domingues, Amy N Moores, Sam Astbury, Christopher Spindloe, Michele C Darrow, Maria Romano, Sarah R Needham, Konstantinos Beis, et al. Solid immersion microscopy images cells under cryogenic conditions with 12 nm resolution. *Communications biology*, 2(1):1–11, 2019.

[36] Siegfried Weisenburger, Daniel Boening, Benjamin Schomburg, Karin Giller, Stefan Becker, Christian Griesinger, and Vahid Sandoghdar. Cryogenic optical localization provides 3d protein structure data with angstrom resolution. *Nature methods*, 14(2):141–144, 2017.

[37] Alberto Diaspro, Giuseppe Chirico, Cesare Usai, Paola Ramoino, and Jurek Dobrucki. Photobleaching. In *Handbook of biological confocal microscopy*, pages 690–702. Springer, 2006.

[38] DM Soumpasis. Theoretical analysis of fluorescence photobleaching recovery experiments. *Biophysical journal*, 41(1):95–97, 1983.

[39] Weixing Li, Simon C Stein, Ingo Gregor, and Jörg Enderlein. Ultra-stable and versatile widefield cryo-fluorescence microscope for single-molecule localization with sub-nanometer accuracy. *Optics express*, 23(3):3770–3783, 2015. URL `https://www.osapublishing.org/oe/fulltext.cfm?uri=oe-23-3-3770&id=311815`.

[40] Alexa fluor 647. URL `https://fluoroprobes.com/product/alexa-fluor-647-nhs-ester/`.

[41] Atto 647n. URL `https://www.atto-tec.com/product_info.php?language=de&info=p114_atto-647n.html`.

[42] KK Banerjee, S Kumar, KE Bremmell, and HJ Griesser. Molecular-level removal of proteinaceous contamination from model surfaces and biomedical device materials by air plasma treatment. *Journal of Hospital Infection*, 76(3):234–242, 2010.

[43] Lukas Sparer. *Building a cryostate for Cryo Fluorescence Microscopy*. PhD thesis, Wien, 2021.

[44] Oleksii Nevskyi, Roman Tsukanov, Ingo Gregor, Narain Karedla, and Jörg Enderlein. Fluorescence polarization filtering for accurate single molecule localization. *APL Photonics*, 5(6): 061302, 2020.

[45] Rainer Kaufmann, Christoph Hagen, and Kay Grünewald. Fluorescence cryo-microscopy: current challenges and prospects. *Current opinion in chemical biology*, 20:86–91, 2014.

[46] Rob Zondervan, Florian Kulzer, Mikhail A Kol'chenk, and Michel Orrit. Photobleaching of rhodamine 6g in poly (vinyl alcohol) at the ensemble and single-molecule levels. *The Journal of Physical Chemistry A*, 108(10):1657–1665, 2004.

[47] Aline Regis Faro, Virgile Adam, Philippe Carpentier, Claudine Darnault, Dominique Bourgeois, and Eve de Rosny. Low-temperature switching by photoinduced protonation in photochromic fluorescent proteins. *Photochemical & Photobiological Sciences*, 9(2):254–262, 2010.

[48] Weixing Li. *Single Molecule Cryo-Fluorescence Microscopy*. PhD thesis, Niedersächsische Staats- und Universitätsbibliothek Göttingen, 2016.

[49] Benji C Bateman, Laura C Zanetti-Domingues, Amy N Moores, Sarah R Needham, Daniel J Rolfe, Lin Wang, David T Clarke, and Marisa L Martin-Fernandez. Super-resolution microscopy at cryogenic temperatures using solid immersion lenses. *Bio-protocol*, 9(22):e3426–e3426, 2019.

[50] Daniele Spehner, Anna M Steyer, Luca Bertinetti, Igor Orlov, Lucas Benoit, Karin Pernet-Gallay, Andreas Schertel, and Patrick Schultz. Cryo-fib-sem as a promising tool for localizing proteins in 3d. *Journal of structural biology*, 211(1):107528, 2020.

6 Appendix: Parameters for ThuderSTORM analysis

Camera setup

Pixel size[nm]	108.0
Photoelectrons per A/D count	4.0
Base level	150.0

Image filtering

Filter	Wavelet filter (B-Spline)
B-Spline order	3
B-Spline scale	4

Approximate localization of molecules

Method	Centroid of connected components
Peak intensity threshold	1.2-1.7*std (Wave.F1)

Sub-pixel localization of molecules

Method	PSF:Integrated Gaussian
Fitting radius[px]	3
Fitting method	Maximum likelihood
Initial sigma[px]	2

Multi-emitter fitting analysis disabled

Additional filtering and drift correction for cryogenic data.

Filter

intensity > 5000 and uncertainty < 50

Density filter

Distance radius	50 nm
Minimum number of neighbors in the radius	5 nm

Drift correction

Fiducial markers	
Max distance	100 nm
Min marker visibility ratio	0.2
Trajectory smoothing factor	0.05